Acute ENaC Stimulation by cAMP in a Kidney Cell Line is Mediated by Exocytic Insertion from a Recycling Channel Pool

Michael B. Butterworth,[1] Robert S. Edinger,[2] John P. Johnson,[2] and Raymond A. Frizzell[1]

[1]Department of Cell Biology and Physiology and [2]Department of Medicine, Renal-Electrolyte Division, School of Medicine, University of Pittsburgh, Pittsburgh, PA 15261

ABSTRACT Acute hormonal regulation of the epithelial sodium channel (ENaC) in tight epithelia increases transcellular Na^+ transport via trafficking of intracellular channels to the apical surface. The fate of the channels removed from the apical surface following agonist washout is less clear. By repetitively stimulating polarized mouse cortical collecting duct (mCCD, $_{MPK}CCD_{14}$) epithelia, we evaluated the hypothesis that ENaC recycles through an intracellular pool to be available for reinsertion into the apical membrane. Short circuit current (I_{SC}), membrane capacitance (C_T), and conductance (G_T) were recorded from mCCD epithelia mounted in modified Ussing chambers. Surface biotinylation of ENaC demonstrated an increase in channel number in the apical membrane following cAMP stimulation. This increase was accompanied by a 83 ± 6% (n = 31) increase in I_{SC} and a 15.3 ± 1.5% (n = 15) increase in C_T. Selective membrane permeabilization demonstrated that the C_T increase was due to an increase in apical membrane capacitance. I_{SC} and C_T declined to basal levels on stimulus washout. Repetitive cAMP stimulation and washout (~1 h each cycle) resulted in response fatigue; ΔI_{SC} decreased ~10% per stimulation–recovery cycle. When channel production was blocked by cycloheximide, ΔI_{SC} decreased ~15% per stimulation cycle, indicating that newly synthesized ENaC contributed a relatively small fraction of the channels mobilized to the apical membrane. Selective block of surface ENaC by benzamil demonstrated that channels inserted from a subapical pool made up >90% of the stimulated I_{SC}, and that on restimulation a large proportion of channels retrieved from the apical surface were reinserted into the apical membrane. Channel recycling was disrupted by brefeldin A, which inhibited ENaC exocytosis, by chloroquine, which inhibited ENaC endocytosis and recycling, and by latrunculin A, which blocked ENaC exocytosis. A compartment model featuring channel populations in the apical membrane and intracellular recycling pool provided an adequate kinetic description of the I_{SC} responses to repetitive stimulation. The model supports the concept of ENaC recycling in response to repetitive cAMP stimulation.

KEY WORDS: cellular traffic • recycle • short-circuit current • capacitance • biotinylation

INTRODUCTION

The epithelial sodium channel (ENaC) is localized at the apical membranes of several epithelia, including lung, colon, sweat gland, salivary glands, taste buds, principal cells of the cortical collecting duct (CCD), and the collecting tubules of mammalian nephrons (Garty and Palmer, 1997; Rossier et al., 2002). In the renal CCD, ENaC constitutes the regulated, rate-limiting entry step in Na^+ reabsorption, and its activity is under strict hormonal control. Abnormalities in ENaC regulation and activity have been linked to a number of human disorders, including hypertension (Liddle's disease), pseudo-hypo aldosteronism (PHA), and cystic fibrosis (Liddle et al., 1963; Hanukoglu, 1991; Mall et al., 2004). The channel is comprised of three homologous subunits: α, β, and γ, whose stoichiometry is thought to conform to the ratio 2α:1β:1γ (Firsov et al., 1996, 1998; Gormley et al., 2003). ENaC exhibits characteristic biophysical properties, including a low single channel conductance (~5 pS), relatively long open and closed times, a high Na^+ to K^+ selectivity ratio (>100:1), and is blocked by the pyrazine diuretic, amiloride, at submicromolar concentrations (Kellenberger and Schild, 2002). The expression and activity of ENaC is regulated by numerous factors, including long (aldosterone) and short (vasopressin, insulin) term hormonal regulation, and sensitivities to flow, stretch, proteases, and altered intra- and extracellular Na^+ concentrations (Palmer, 1992; Garty and Palmer, 1997).

In many ENaC-expressing tissues and model epithelia, a rapid stimulation of sodium transport is elicited by vasopressin through increases in intracellular cAMP levels and PKA activation (Benos et al., 1995; Garty and Palmer, 1997; Els and Butterworth, 1998; Ecelbarger et al., 2001; Snyder, 2002). Some debate exists regarding the mechanism by which vasopressin increases Na^+ transport (Rossier, 2002); that is, increased open

Correspondence to Michael B. Butterworth: michael7@pitt.edu

Abbreviations used in this paper: BFA, brefeldin A; CCD, cortical collecting duct; CHX, cycloheximide; ENaC, epithelial sodium channel; LatA, latrunculin A; TGN, trans-Golgi network.

J. Gen. Physiol. © The Rockefeller University Press • 0022-1295/2005/01/81/21 $8.00
Volume 125 January 2005 81–101
http://www.jgp.org/cgi/doi/10.1085/jgp.200409124

probability (P_o) or increased apical membrane channel number (N). Nevertheless, several studies have suggested that the acute (sec–min) increase in Na^+ transport is the result of regulated insertion of ENaC-containing intracellular vesicles into the apical membrane (increased N) (Erlij et al., 1999; Snyder, 2000; Weisz et al., 2000; Butterworth et al., 2001; Morris and Schafer, 2002; Planes et al., 2002). The residence time of channels at the apical surface is regulated by removal and degradation processes, which are initiated by the binding of Nedd4-2 to the cytoplasmic COOH termini of the ENaC subunits. All three subunits contain a proline rich region (PPXYXXL), which binds Nedd4 to target ENaC for ubiquitin-dependent internalization and degradation (Goulet et al., 1998; Abriel et al., 1999; Farr et al., 2000; Staub et al., 2000; Malik et al., 2001). Mutations in the PY motifs at the subunit COOH termini of β- and γ-ENaC result in increased ENaC residency in the plasma membrane and a constitutive increase in Na^+ transport. Although polyubiquitination is often a marker for proteosomal degradation, monoubiquitination is also associated with endocytosis and recycling of plasma membrane proteins such as the epidermal growth factor (EGF) receptor (Sorkin, 2001; Dikic, 2003). Thus, the extent to which ENaC retrieved from the apical surface is subjected to degradation versus recycling is unclear.

To characterize the acute regulation of ENaC by cAMP, mouse CCD cells cultured on permeable supports were repeatedly stimulated to fatigue the short-circuit current (I_{SC}) response and identify the mechanisms regulating apical ENaC activity. We show that PKA activation resulted in the insertion of ENaC subunits into the apical surface, which results in cAMP-induced increases in I_{SC} and epithelial capacitance (C_T). On agonist removal, both I_{SC} and C_T declined to basal levels, and subsequently the cells were able to respond to additional rounds of stimulation. By blocking protein biosynthetic pathway or membrane trafficking pathways, evidence was provided for a subapical pool of recycling channels. We propose that distinct ENaC populations in CCD epithelia account for constitutive and regulated Na^+ transport and that the acute stimulation of Na^+ transport is due primarily to insertion of ENaC from a tightly regulated channel recycling pool.

MATERIALS AND METHODS

Cell Culture

The $mpkCCD_{c14}$ cells (provided by A. Vandewalle and M. Bens, Institut National de la Santé et de la Recherche Médicale, Paris, France) were grown in flasks (passage 30–40) in defined medium as described previously (Vinciguerra et al., 2003). Growth medium was composed of equal volumes DMEM and Ham's F_{12}, 60 nM sodium selenate, 5 μg/ml transferrin, 2 mM glutamine, 50 nM dexamethasone, 1 nM triiodothyronine, 10 ng/ml epidermal growth factor, 5 μg/ml insulin, 20 mM D-glucose, 2% vol/vol FCS, and 20 mM HEPES (Invitrogen, GIBCO BRL, Sigma-Aldrich), pH 7.4, at 37°C in 5% CO_2/95% air atmosphere. The medium was changed every second day. For all electrophysiological experiments, the CCD cells were subcultured onto permeable filter supports (0.4 μm pore size, 0.33 cm^2 surface area; Transwell, Corning Costar). Cells were kept on filters for at least 7 d in defined medium which was changed every second day. Typically after 7 d, a confluent transporting cell monolayer had developed that could be assessed by recording open circuit voltage and transepithelial resistance using "chopstick" electrodes (Millipore). At least 24 h before use in any investigation, medium incubating cells on filters was replaced with a minimal medium (without drugs or hormones) that contained only DMEM and Ham's F_{12}.

Standard I_{SC} Current Recordings

Cells cultured on filter supports were mounted in modified Costar Ussing chambers, and the cultures were continuously short circuited with an automatic voltage clamp (Department of Bioengineering, University of Iowa, Iowa City, IA). Transepithelial resistance was measured by periodically applying a 2.5-mV bipolar pulse and calculated using Ohm's law. The bathing ringers solution was composed of 120 mM NaCl, 25 mM $NaHCO_3$, 3.3 mM KH_2PO_4, 0.8 mM K_2HPO_4, 1.2 mM $MgCl_2$, 1.2 mM $CaCl_2$, and 10 mM glucose. Chambers were constantly gassed with a mixture of 95% O_2/5% CO_2 at 37°C, which maintained the pH at 7.4. To facilitate chamber washes, the bases of both chamber compartments were connected to a peristaltic pump, in order to control volume flow rate, with fluid removed from the top of the chamber. At the minimum, a fivefold volume exchange (25–30 ml) was performed to wash out the chamber, and in some cases, this was increased (see below) to ensure sufficient removal of agonist or other compounds. As the cells were sensitive to changes in pressure, flow, and temperature, the chamber solutions were only exchanged during wash periods with no flow at steady states. A disruption was always noted in the recorded traces during basolateral chamber wash periods, but currents returned to prewash levels at the end of the fluid exchange. Similar transients were observed when solution of the same composition was exchanged in the basolateral chamber. A typical stimulation cycle lasted 1 h and involved the addition of 10 μM forskolin basolaterally, which produced a maximum I_{SC} stimulation after 20–30 min; forskolin was washed from the basolateral side of the chamber and current declined back to basal levels within 30 min. To determine the net Na^+ transport through ENaC, 10μM amiloride was added to the apical cell surface at the end of each experiment.

Simultaneous I_{SC}, Capacitance, and Impedance Recordings

The same modified Ussing chambers were used to record simultaneous I_{SC} and C_T traces. The voltage clamp and recording system used to acquire data were designed and constructed by W. Van Driessche (Katholieke Universiteit, Leuven, Belgium) and have been described in detail previously (Erlij et al., 1999; Weber et al., 1999). In brief, hardware for C_T measurements used two Digital Signal Processing (DSP) boards (Model 310B; Dalanco Spry) with one board used to record transepithelial conductance (G_T) and short-circuit current (Isc) and the second, C_T. Due to the requirement to generate multiple sine waves in order to obtain simultaneous measurements, the system only updated recorded values every 7 s. As stimulation events occurred over tens of minutes, this was not limiting. Continuous C_T values were calculated from imposed voltage sine waves of frequencies 2, 2.7, 4.1, 5.4, and 8.2 kHz. The 4.1-kHz trace is presented in all C_T figures. Impedance analysis was performed at steady states by simultaneously imposing 78 sine waves to the command input of the

voltage clamp and analyzed as previously described (Weber et al., 1999). The Nyquist plot obtained from the impedance spectra exhibited only one semicircle, which is presumed to reflect the apical membrane capacitance. The relative contribution of each membrane to C_T was determined by selectively permeabilizing each membrane with ionophores (see below). It was not practical to utilize ionophores in long term studies performed here, and as it could be demonstrated by permeabilization studies that the capacitance changes were the result of alterations in C_A alone (see below), C_T recordings could be assumed to reflect changes in C_A (see also Erlij et al., 1999; Weber et al., 1999).

Membrane Permeabilization

To isolate apical and basolateral membranes electrically, bathing ringers solutions were kept identical on both sides of the chamber and increasing doses of nystatin (25, 50, 75, 100 μM; Sigma-Aldrich) were added to either side to incrementally permeabilize the membrane and assess the effect by monitoring I_{SC}, G_T, and C_T. To investigate the effect of forskolin stimulation on capacitance changes in either membrane, 100 μM nystatin was used, as full membrane permeabilization was achieved at this concentration.

Surface Biotinylation

CCD cells cultured on 75-mm diameter filter supports (Transwell) were washed (5 min) with ice-cold PBS with agitation on ice to remove growth media. The apical membrane was biotinylated using 0.5 mg/ml S-S-biotin (Pierce Chemical Co.) in borate buffer (85 mM NaCl, 4 mM KCl, 15 mM $Na_2B_4O_7$, pH 9) for 20 min. The basolateral surface was incubated in growth medium containing FBS to prevent biotinylation. Biotinylation was quenched by adding a double volume FBS-containing medium on the apical surface. Monolayers were then washed three times with ice-cold PBS with agitation on ice, and the cells were harvested. Cells were lysed in cell lysis buffer (0.4% DCA, 1% NP-40, 50 mM EGTA, 10 mM Tris-Cl, pH 7.4) at room temperature for 10 min. Protein concentration of the post nuclear supernatant was determined, and 200 μg of protein was combined with a streptavidin bead slurry (Pierce Chemical Co.) and incubated overnight at 4°C. Samples from the streptavidin beads were collected in 2× sample buffer containing 10% β-mercaptoethanol and incubated for 20 min at room temperature. Samples were heated at 95°C for 3 min, separated by SDS-PAGE, and subjected to Western blot analysis with the appropriate antibodies and visualized using chemiluminescence (Perkin-Elmer). To verify that intracellular proteins were not biotinylated during the experimental procedure, biotinylated samples collected from unstimulated and forskolin-stimulated epithelia were separated by SDS-PAGE as described, and blotted for actin.

Western Blot Controls

To examine the specificity of the antibodies used, 15 μg of the immunizing peptides (where available) were preincubated with the relevant sera for 1 h at 37°C before applying to resolved Western blots. The protein was separated by SDS-PAGE, transferred to nitrocellulose, and subjected to Western blot analysis as described.

Protein Synthesis Assays

To determine the effect of cycloheximide (CHX) on protein production, CCD cells cultured on 6 well structures (Transwell) were treated with or without 200 μg/ml CHX for 15 min. The cells were washed once with 1 ml of DME media lacking methionine and cysteine (Met/Cys; ICN Biomedicals) and starved for Met and Cys in the same media for 15 min before addition of 50–100 μCi of [^{35}S]Met/Cys (New England Nuclear, PerkinElmer) and pulsed for 15 min. CHX-treated cells were treated the same way except that media was supplemented with 200 μg/ml CHX. The cells were washed and isolated as described above. Equal amounts of lysate were separated by SDS-PAGE. Total radioisotope incorporation was quantitated from the dried gel using a phosphoimager (Bio-Rad Laboratories).

Transient GFP-Endo Transfection

The pEGFP-Endo reporter vector, which encodes a fusion protein containing the human RhoB GTPase, was obtained from BD Biosciences (CLONTECH Laboratories, Inc.). The vector was transiently transfected into mCCD cells cultured on glass using lipofectamine 2000 (Invitrogen) according to manufacturer's protocol. Cells were used 24 h post-transfection in imaging studies to localize early endosomal compartments.

Microscopic Image Capture and Processing

All fluorescent images were acquired on a Nikon Diaphot-300 epifluorescent microscope using a 40× 1.4 N.A. objective and equipped with a Hamamatsu C4742-95 CCD camera. Images were processed using Metamorph (Universal Imaging Corp.) with adjustments made to only contrast and brightness (phalloidin staining) or simple nearest neighbor deconvolution followed by brightness adjustment (GFP-Endo).

Reagents, Fluorophores, and Antibodies

Brefeldin A (BFA) and Latrunculin A (LatA), which were reconstituted in DMSO at 1,000 times stock solutions, and Alexa Fluor-568 phalloidin were obtained from Molecular Probes. CHX (500 mg/ml stock solution in DMSO), arginine-vasopressin (100 IU/ml stock), benzamil, nickel chloride, chloroquine, and Hoechst nuclear stain were obtained from Sigma-Aldrich. Forskolin (10 mM stock in ethanol) was obtained from Calbiochem (CN Biosciences). DMSO and ethanol, used as vehicles, had no significant effect on recorded I_{SC} when added at 1:1,000 dilution alone (not depicted). ENaC antibodies were donated by K. Peters (Department of Cell Biology, University of Pittsburgh; α-ENaC) and M. Knepper (Laboratory of Kidney and Electrolyte Metabolism, National Heart, Lung, and Blood Institute, National Institutes of Health, Bethesda, MD; β-ENaC) or were commercially obtained for γ-ENaC (Abcam).

Data Analysis and Modeling Software

Summarized data are presented as mean and standard error (Sigmaplot 2000; SPSS). Simple linear regression fits were performed using Sigmaplot. Object-based modeling software (Model Maker V4; Model Kinetix) was used to construct a compartmental model to describe channel trafficking events. Traces for the kinetic events were obtained by using the built-in integration engines provided in the software and integrating the functions over desired time lengths.

RESULTS

cAMP Stimulation Increases I_{SC} and C_T

Fig. 1 illustrates typical short-circuit current (I_{SC}) and transepithelial capacitance (C_T) traces from CCD epithelia stimulated with 10 μM forskolin. Basal I_{SC} increased, after an initial dip due to K^+ efflux (the small I_{SC} decline was eliminated in the presence of 5 mM

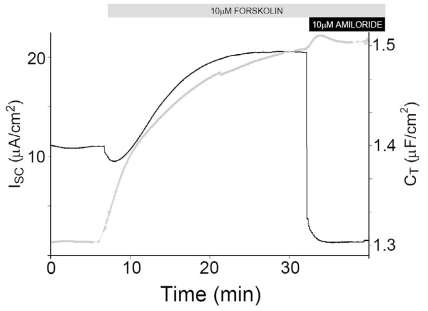

FIGURE 1. mCCD epithelia response to forskolin. (A) Typical I_{SC} and C_T responses to 10 μM basolateral forskolin addition. Amiloride (10 μM) added apically at the I_{SC} peak demonstrated that >90% of recorded I_{SC} was I_{Na} and had little effect on recorded C_T.

$BaCl_2$; unpublished data), to a value almost twofold greater than baseline over a 25-min time course. The increase in I_{SC} was immediately preceded, and then paralleled, by an increase in C_T. Addition of 10 μM amiloride reduced the I_{SC} by >90%, demonstrating that the majority of the transepithelial current was ENaC-mediated I_{Na}. Amiloride had no significant effect on C_T, indicating that the measured capacitance was not influenced by changes in transepithelial current or conductance. A similar response was observed when epithelia were stimulated with arginine vasopressin (AVP), however a larger stimulation, which was more readily reversed, was recorded with forskolin (unpublished data). As a result, all subsequent experiments made use of forskolin to elicit cAMP-mediated increases in I_{Na}.

Forskolin Increases Apical Membrane ENaC Density

To investigate the basis of the increased I_{Na}, apical biotinylation was performed on filter-cultured CCD epithelia using identical stimulation conditions. Increases in all ENaC subunits accessible to biotin labeling at the apical surface were observed following a 30-min forskolin stimulation (Fig. 2 A, with densitometric quantitation of forskolin-induced fold increases in signal presented beneath the blot for each subunit). This indicated that the increase in I_{SC} was due, in part, to insertion of channel subunits that increased apical ENaC density. As a control, no intracellular biotin labeling was observed when samples were probed for actin (Fig. 2 B). Preincubation of the anti-α and γ ENaC antibodies with immunizing peptide for control purposes eliminated the specific signal in the whole cell lysate (Fig. 2, C and D), the molecular weight of subunits detected following biotinylation did not represent all the bands detected in whole cell lysates (Fig. 2 C). This may be due to detection of mature or processed forms of these subunits at the apical surface (see DISCUSSION and Hughey et al., 2004b).

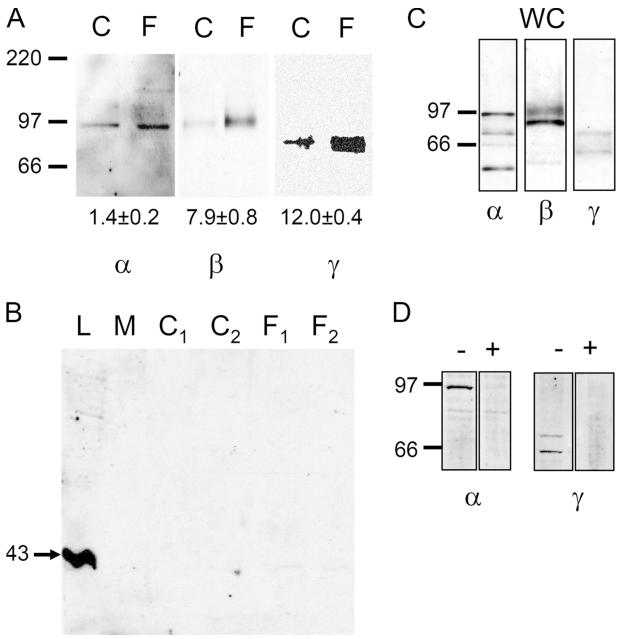

FIGURE 2. Apical surface biotinylation. (A) Forskolin stimulation (30 min) resulted in increased ENaC available for biotinylation at the apical surface as observed in subsequent Western blots from paired CCD epithelia. C = control unstimulated, F = 10 μM forskolin stimulated. Densiometric quantitation of the fold increase in surface labeling is presented beneath each blot for α-, β-, and γ-ENaC subunits (n = 3). (B) Actin control for biotinylated samples demonstrates that no observable signal can be detected in control (two separate samples C_1 and C_2) or forskolin-stimulated (F1 and F2) biotinylated samples (L = whole cell lysate as positive control, M = lane for molecular weight standards). (C) Western blot for whole cell lysate obtained from control mCCD epithelia cultured on filter supports. (D) Western blot of peptide competition controls for anti α- and γ-ENaC antisera demonstrate specific resolved bands in the absence of immunizing peptide (−) are competed when antisera was incubated with the immunizing peptide (+).

Forskolin Increases Apical Membrane Capacitance

To better interpret the C_T measurements, the epithelium was modeled as series RC circuits corresponding to the apical and basolateral membranes, shunted by a paracellular resistance. In this standard lumped model, C_T is described by

$$\frac{1}{C_T} = \frac{1}{C_A} + \frac{1}{C_B} \quad (1)$$

(Weber et al., 1999; Erlij et al., 1999).

In polarized A6 epithelia, C_B is at least six times larger than C_A so that the relative contribution of C_B to transepithelial capacitance is small (Erlij et al., 1994, 1999; Wills et al., 1992). Accordingly, changes in C_T primarily reflect changes in C_A (Weber et al., 1999; Paunescu and Helman, 2001a,b).

The individual membrane contributions to the forskolin-induced ΔC_T across CCD epithelia were evalu-

ated using selective membrane permeabilization with the addition of 25–100 μM nystatin to either the apical or basolateral bath. Incremental apical nystatin additions were used to resolve the basolateral membrane electrically while simultaneously monitoring I_{SC}, conductance, impedance, and capacitance to determine the point at which the apical surface was effectively permeabilized. The dose-dependent progression to an isolated basolateral membrane is demonstrated by the impedance plots shown in Fig. 3 A. Apical permeabilization as illustrated for a typical experiment in Fig. 3 B resulted in (a) effective elimination of the apical membrane resistance, reflected by a decrease in R_T from ~3,000 Ω.cm^2 to ~400 Ω.cm^2, (b) an increase in I_{SC}, which was blocked by ouabain (not depicted), to a value six to sevenfold greater than the basal current, this ouabain-sensitive current is due to cation transport of the basolateral Na^+/K^+ ATPase and has been previously demonstrated for polarized epithelial cells (Fujii and Katz, 1989; Rokaw et al., 1996; Ito et al., 1999), and (c) an increase in C_T to a value about fourfold higher than that observed for the intact epithelium. The C_T value following apical nystatin treatment verifies the assumption that the basal surface area was far larger than that of the apical membrane, so that in the intact epithelium, C_A dominates the C_T measurement. Four similar treatments produced nystatin-induced increases in C_T that averaged 4.15 ± 0.12-fold. Substituting the capacitance values observed in Fig. 3 B into Eq. 1 (above), a calculated C_A = 1.25 μF/cm^2 is obtained, which is similar to C_T values of 1.29 ±0.03 μF/cm^2 recorded in control, unstimulated epithelia (n = 15). Moreover, in the presence of apical nystatin, there was no significant change in recorded capacitance in response to forskolin, suggesting that a basolateral capacitance change did not contribute significantly to the forskolin-induced increase in C_T. Conversely, when the basolateral membrane was permeabilized, apical capacitance increased 14 ± 2% (n = 4), which was not significantly different from the C_T increase of 15 ±1.5% (n = 15) observed in control, unpermeabilized epithelia (Fig. 3 C).

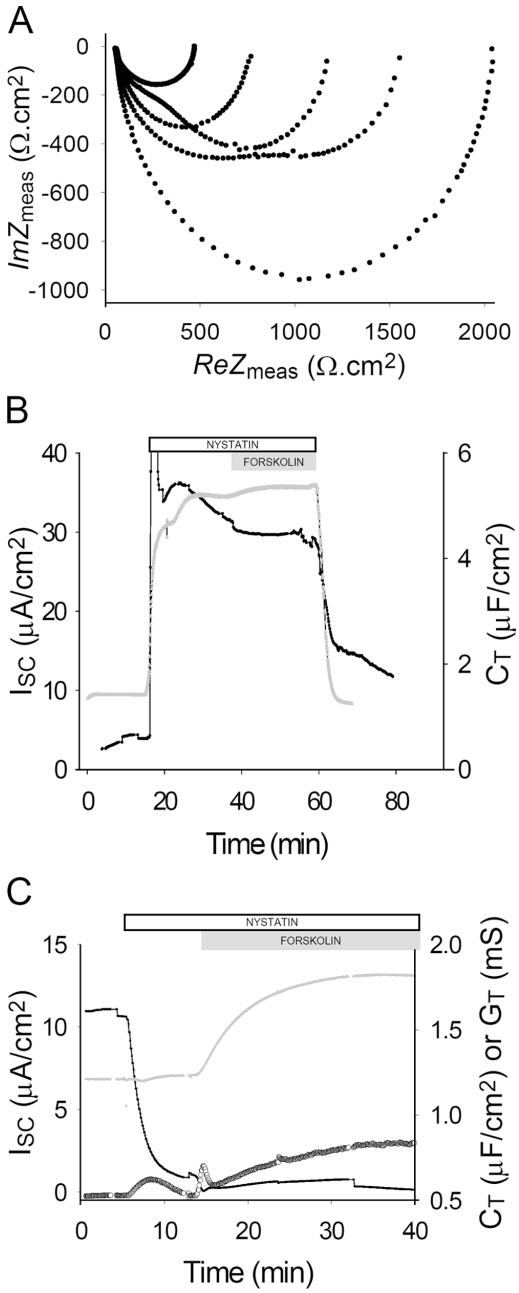

FIGURE 3. Membrane permeabilization. (A) Nyquist plots from a CCD epithelium to which increasing concentrations of apical nystatin was added. From an unpermeabilized state, a single impedance locus (one semicircle) transitioned through two loci until only one locus corresponding to the basolateral membrane was observed (at 100 μM nystatin). (B) Time course of I_{SC} (black) and C_T (gray) plots in response to apical nystatin addition (white bar). Small changes in recorded basolateral capacitance with forskolin (gray bar) were insufficient to account for observed ΔC_T changes. (C) A similar plot (as in B) for basolateral permeabilization exhibits a C_T response to 10 μM basolateral forskolin addition similar to unpermeabilized epithelia. I_{SC} decreased due to removal of transepithelial driving force. Small drift in G_T (open circles) indicates that transepithelial resistance remained fairly constant.

Repetitive cAMP Stimulation Causes I_{SC} Response Rundown

The I_{SC} and C_T responses to repetitive forskolin challenges were examined in an attempt to determine whether this technique could be used to evaluate the fate of inserted channels following washout of the cAMP agonist. Typical I_{SC} and C_T traces from one such experiment are presented in Fig. 4 A. With each successive stimulation–recovery cycle (~1 h each), the forskolin-induced ΔI_{SC} diminished. The resulting ΔI_{SC} decay is plotted in Fig. 4 B, where the slope of the linear regression fit indicates a loss of ~10% of the ΔI_{SC} with each response (slope = −11.33, r^2 = 0.99). Plotted on

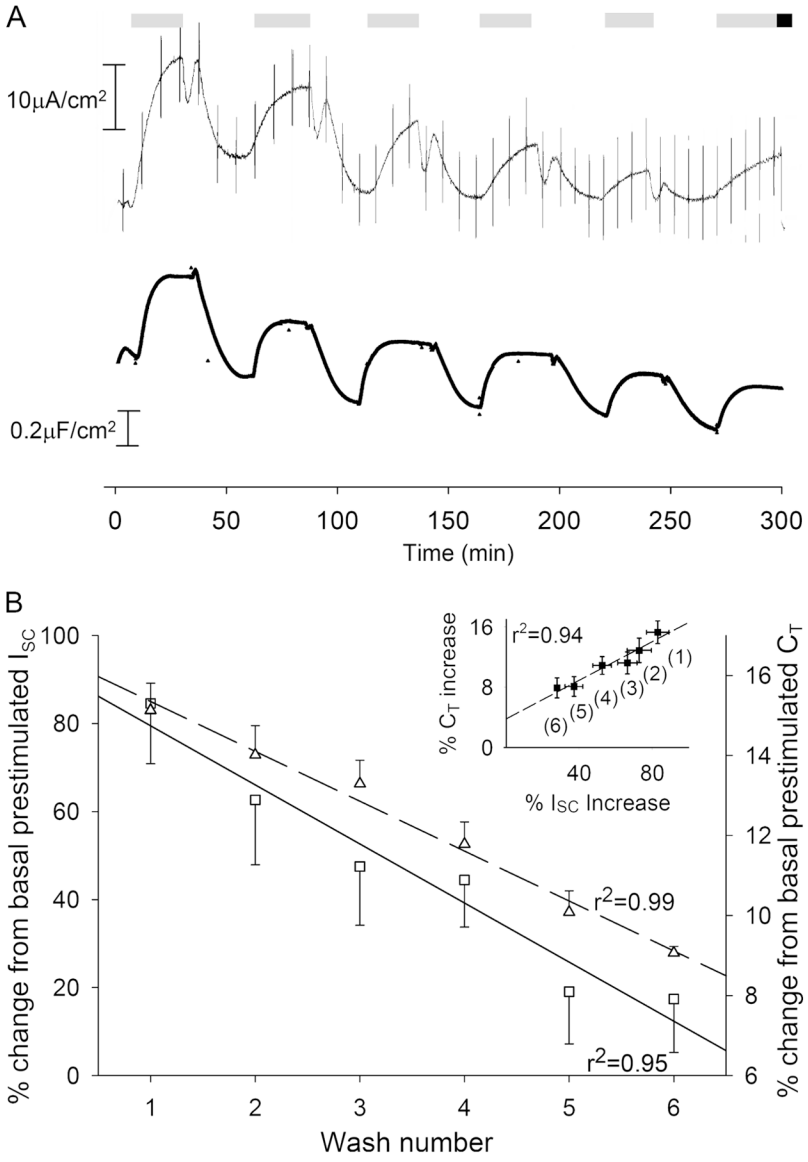

FIGURE 4. Repetitive stimulation and ΔI_{SC} rundown. (A) Time course of I_{SC} and C_T plot with repeated basolateral forskolin (gray bar) stimulation and washout. Note the artifact in I_{SC} where forskolin is washed from the basolateral chamber (see Fig. 6 C). (B) Decline in forskolin response (I_{SC}, △; C_T, □) as a percentage of basal values. Fitted linear regression (with associated r^2 value) is plotted for each parameter (n = 6–31 for each data point). Inset graph plots ΔC_T vs. ΔI_{SC} as percentage change for each stimulation (parenthesis), indicating that declines in I_{SC} and C_T are correlated.

separate axes, the change in forskolin-induced C_T also fell (slope = −1.47, r^2 = 0.95). By plotting $\%\Delta I_{SC}$ vs. $\%\Delta C_T$ for each stimulation cycle (Fig. 4 B, inset), it is clear from the single regression analysis that the decline in ΔI_{SC} was correlated with the decline in ΔC_T.

Retrieved ENaC Recycles to the Apical Membrane on Restimulation

From these data, it is apparent that these cells respond repeatedly to forskolin, which elicits an insertion of channels into the apical membrane. To determine whether these responses involve insertion of recycled channels, ENaC-dependent I_{SC} was blocked in two ways. Partial, irreversible inhibition of ENaC-Na^+ currents expressed in oocytes by $NiCl_2$ has been demonstrated previously (Sheng et al., 2002). Addition of 20 mM $NiCl_2$ apically resulted in a significant 26.1 ± 4.5% (n = 5) inhibition in forskolin-stimulated I_{SC} (Fig. 5 A), which could not be reversed by apical washing (not depicted). Restimulation of epithelia following a 30-min recovery period produced a significantly reduced I_{SC} response to forskolin compared with uninhibited controls, suggesting that channels that were inserted into the membrane were those previously inhibited by $NiCl_2$ (Fig. 5 B).

Similarly, 10 μM benzamil was used to selectively block channels that reside in the apical membrane. Benzamil is more potent than amiloride, and it is not readily reversible, due to a much slower dissociation rate relative to that of amiloride (Kleyman et al., 1986; Kellenberger et al., 2003) and the fact that it was not washed out of the apical membranes of mCCD epithelia mounted in the Ussing chambers (compare with amiloride washout; see Fig. 6, D–F). Benzamil was added at different times during the stimulation protocol to block membrane-res-

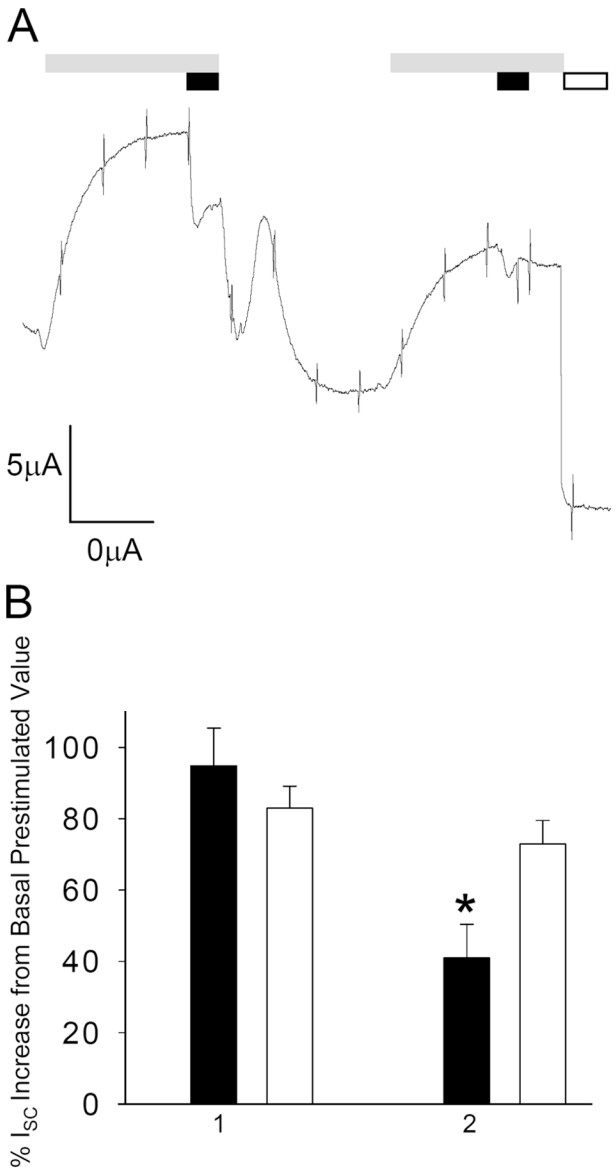

FIGURE 5. $NiCl_2$ block of I_{SC}. (A) A representative I_{SC} trace demonstrates that the addition of 20 mM $NiCl_2$ (black bar) to the apical bathing solution at the peak of the 10 μM forskolin stimulation (gray bar) results in an irreversible inhibition of ENaC current (note no recovery of current on washout of $NiCl_2$). Following stimulus washout, restimulated I_{SC} response is significantly reduced and a second $NiCl_2$ addition (black bar) fails to inhibit the previously blocked ENaC. (white bar, addition of 10 μM amiloride). (B) A normalized summary of six experiments performed in the same manner as A demonstrates that initial (1 = first stimulation) unblocked response (black bar) to forskolin stimulation is not significantly different from control experiments (white bar). Following irreversible ENaC block by $NiCl_2$ (black bar), a subsequent stimulation (2 = second stimulation) is significantly smaller when compared with control epithelia (white bar).

ident ENaC. Examples of I_{SC} traces from two such experiments are presented in Fig. 6 (A and B). As a control, the cells were initially subjected to one round of forskolin stimulation. In Fig. 6 A, benzamil was added at baseline following forskolin washout, while in Fig. 6 B, it was added at the peak of the next forskolin response. After 5 min incubation with benzamil, the apical chamber was washed extensively (10-fold volume exchange as opposed to the usual fivefold) to completely remove the blocker from the bath. In Fig. 6 A, epithelia were then restimulated with forskolin after benzamil had blocked the basal current. The observed increase in I_{SC} was therefore due to insertion of channels from an intracellular pool that was inaccessible to apical benzamil blockade. The increase in I_{SC} supports the biotinylation data (Fig. 2), which detected additional ENaC subunits at the apical surface following forskolin stimulation. In Fig. 6 B, channels were blocked by benzamil addition at the peak of the forskolin response. After forskolin washout, and allowing sufficient time to ensure retrieval of channels from the apical surface (30 min; see Fig. 4 A), the cells were restimulated. The I_{SC} response to forskolin was essentially abolished, suggesting that if channels were recruited to the apical surface, they were those that had been blocked by benzamil during the previous stimulation. The control epithelium (Fig. 6 C) received two control washes (apical and basal) and were then stimulated by forskolin after 2 h to verify that the wash protocol and extended short circuiting had no adverse effects on the cells or their forskolin response. Fig. 6 G summarizes the results from five experiments like those presented in Fig. 6 (A and B). The data demonstrate that channels blocked by benzamil at the peak of forskolin stimulation comprise the majority of channels inserted upon restimulation.

Benzamil Block Does Not Disrupt Trafficking

To evaluate the influence of benzamil on membrane trafficking, C_T was recorded from cells subjected to the protocol of Fig. 6 B. Note that even when the I_{SC} is almost completely blocked (Fig. 7 A), the C_T response to forskolin was similar to that observed in control epithelia. This indicates that channel blockade did not influence the trafficking processes that result in an increased ENaC delivery to the cell surface in response to forskolin. This result is consistent with the lack of effect of amiloride on C_T presented in Fig. 1.

Newly Synthesized ENaC Is Not Essential for the cAMP Response

To determine whether newly synthesized channels were required for repeated rounds stimulation, epithelia were treated with 200 μg/ml CHX for 30 min before the first forskolin stimulation to block protein synthesis and channel progression through the biosynthetic pathway. The efficacy of CHX disruption of protein production was determined by [^{35}S]Met/Cys incorporation in control and CHX-treated epithelia as described in MATERIALS AND METHODS. Phosphoimager radioactive counts for control epithelia were 13,570 ± 1,770 (n =

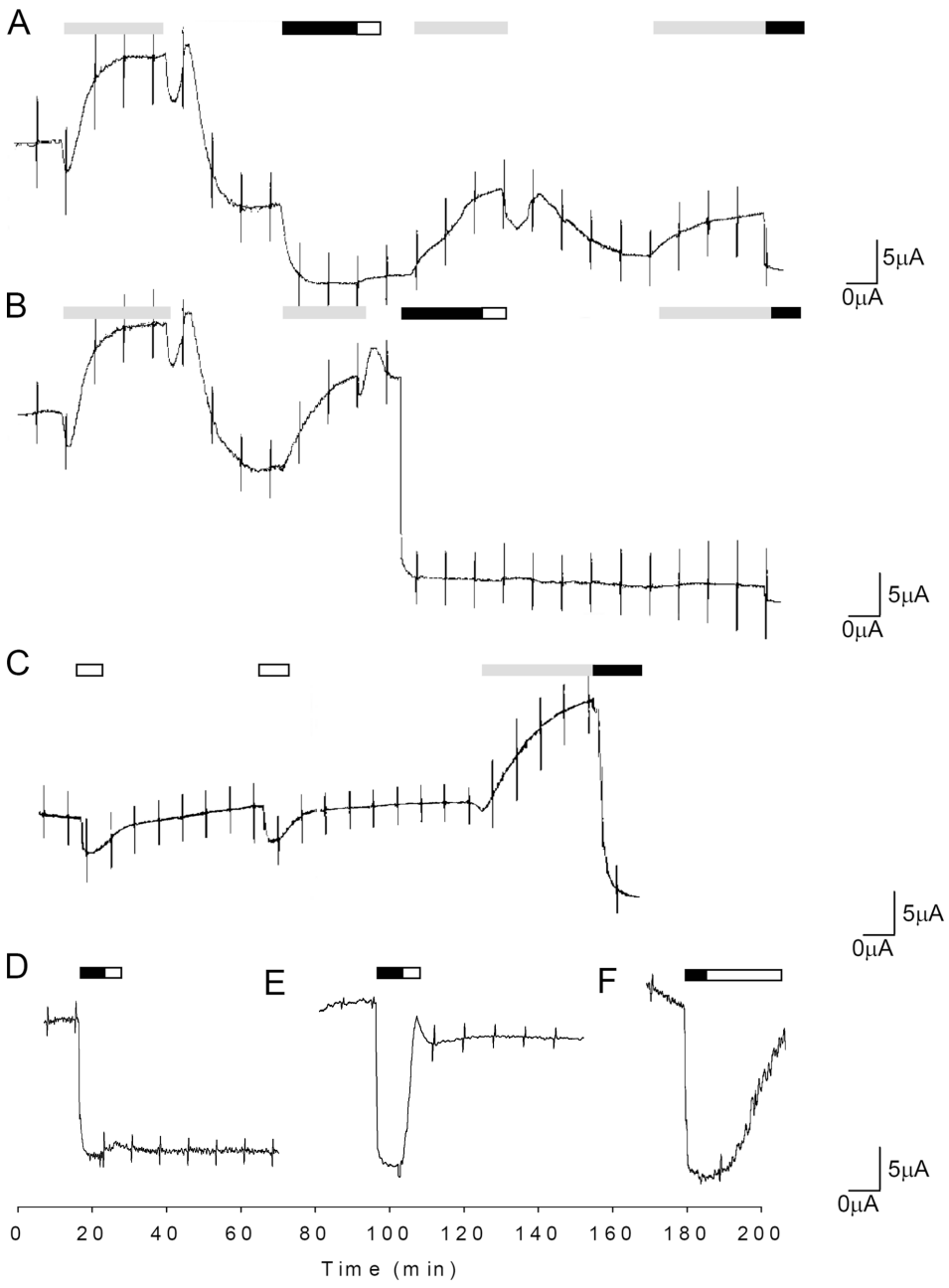

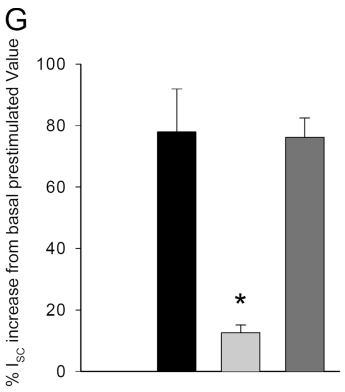

FIGURE 6. Benzamil block of I_{SC}. (A) I_{Na} was blocked by 10 μM benzamil (black bar), which was added to the apical chamber after currents had returned to baseline following an initial forskolin (gray bar) stimulation (basal I_{SC} block). Following an extensive apical wash (white bar), basolateral forskolin addition (gray bar) stimulated I_{SC}, indicating ENaC insertion from a pool inaccessible to block by apical benzamil addition. (B) Cells were subject to two rounds of forskolin stimulation (gray bar). Benzamil (black bar) was added at the I_{SC} peak of the second forskolin stimulation to block all channels present in the apical surface including those delivered by vesicle insertion. Both benzamil and forskolin were washed out and cells were restimulated after sufficient time had elapsed to ensure channel retrieval had occurred (see timing for multiple stimulation in Fig. 4). No additional I_{SC} stimulation was noted following a third forskolin addition. (C) Control epithelium received two sham washes (white bar), illustrating the I_{SC} wash artifact, followed by forskolin stimulation (gray bar) at 120 min. (D) Benzamil addition (black bar) to basal current inhibited I_{Na}, which did not recover significantly following an apical wash (white bar) using the same fluid volume as for washes performed in A and B. (E) Basal current was blocked by apical addition of 10 μM amiloride (black bar). I_{SC} was restored close to baseline values following apical wash using the same fluid volume as for washes in A and B, indicating that this blocker was more readily reversible than benzamil. (F) I_{SC} was blocked by 10 μM apical benzamil addition (black bar). The apical chamber was then washed continuously until baseline current had been restored (white bar) after >15 min of fluid exchange, indicating that benzamil was a poorly reversible blocker in this experimental setup. (G) Summary of ΔI_{SC} percent increase from basal currents for five experiments performed in the same way as either A or B. Epithelia in which current was blocked before stimulation (black bar) responded by increasing current by 7.05 ± 3.8 μA/cm², which was not statistically different from the 9.2 ± 1.0 μA/cm² increase in control cells (dark gray bar) (n = 30). When benzamil was added at the peak of the forskolin response (light gray bar) and cells were restimulated, the current increase of 0.9 ± 0.5 μA/cm² was significantly lower than controls (*, $P < 0.05$).

6) compared with CHX-treated cells, which had only 1,120 ± 98 (n = 6), representing a reduction of ~92% in radiolabeled protein. This demonstrated that protein production was essentially eliminated by treatment with 200 μg/ml CHX. CHX remained in the bathing solutions for the duration of the experiment. The CHX-treated cells were able to respond to repetitive stimulation, as observed for control epithelia. However, the

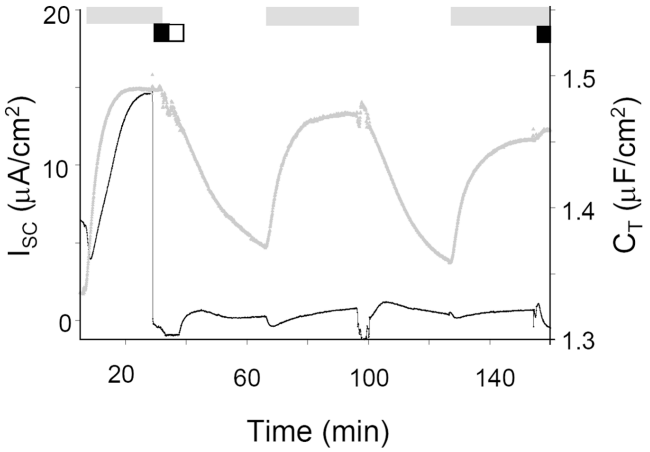

FIGURE 7. Capacitance response in the presence of benzamil. Simultaneous I_{SC} (black trace) and C_T (gray trace) recordings illustrate that the reduced forskolin response was not due to a failure to insert membrane, as C_T changes with repetitive stimulation were unaffected (forskolin and benzamil addition indicated by bars as in Fig. 6 A).

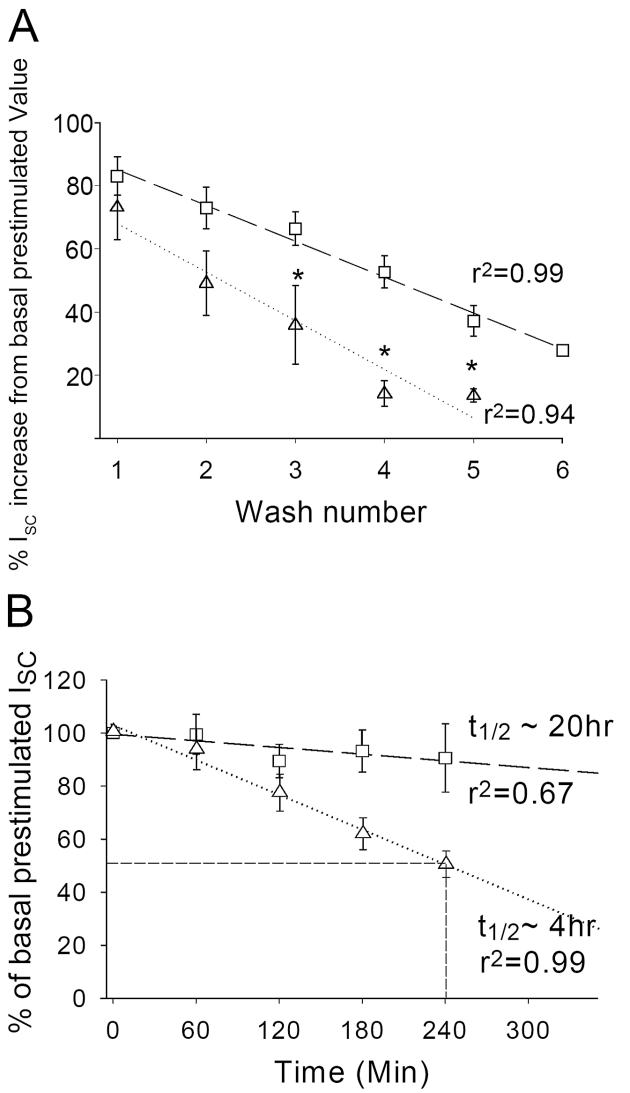

FIGURE 8. CHX effects on I_{SC}. (A) ΔI_{SC} decay with rounds of stimulation plotted for control (□) and CHX-treated (△) epithelia ($n > 4$). Fitted regression slopes indicated a loss in response of 11.3% and 15.4% for control and CHX epithelia, respectively (*, $P < 0.05$). (B) The decline in basal current over time is plotted for control (□) and CHX-treated (△) epithelia. Fitted linear regression and $t_{1/2}$ presented for each curve. Points are mean and SEM ($n \geq 4$).

ΔI_{SC} response ran down more quickly than under control conditions, resulting in a loss of ~15% of ΔI_{SC} per stimulation cycle (Fig. 8 A). From these data, it would appear that newly synthesized ENaC does not make up the majority of channels inserted into the apical membrane in response to repetitive forskolin stimulation; rather, synthesis augments the recycling pool by ~5% per cycle, since the decline in ΔI_{SC} was slightly faster after CHX treatment. The effect of prolonged CHX treatment on basal, unstimulated currents is presented in Fig. 8 B. From the fit, control CHX-untreated epithelia had a basal current half-life of >20 h, whether they were repeatedly stimulated or not. In CHX-treated epithelia, the basal current decay was more rapid (current half-life ~4 h). The rundown in current under control conditions likely reflects fatigue due to the extended duration of the experiments. Nevertheless, by blocking channel synthesis, an indication of the functional half-life of channels inserted into the apical membrane in response to forskolin has been obtained, and these data were used to model apical ENaC recycling (see below).

Brefeldin A Disrupts ENaC Recycling

The effect of disrupting channel trafficking from the trans-Golgi network (TGN) to the plasma membrane was examined using BFA. A typical I_{SC} trace from a BFA-treated CCD epithelium (Fig. 9 A) demonstrates that the initial forskolin response was not impaired, but that subsequent stimulations were markedly reduced. Data obtained for the second I_{SC} response to forskolin in the presence of BFA are summarized in Fig. 9 B.

The effect of BFA was reversible, but the time taken to restore full function was dependent on the initial dose and incubation time (unpublished data). Full responsiveness was reestablished in cells receiving 5 μg/ml BFA after two stimulation cycles, or ~2 h. The effect of BFA on ΔC_T is presented in Fig. 9 C. The diminished ΔI_{SC} results from an inability of the cells to deliver ENaC-containing vesicles back to the apical surface since the forskolin-induced ΔC_T response to a second stimulation was significantly reduced by BFA.

Chloroquine Blocks ENaC Endocytosis

The effect of inhibiting ENaC endocytosis from the apical surface was investigated by treating CCD epithelia with 100 μM chloroquine. Chloroquine has been used

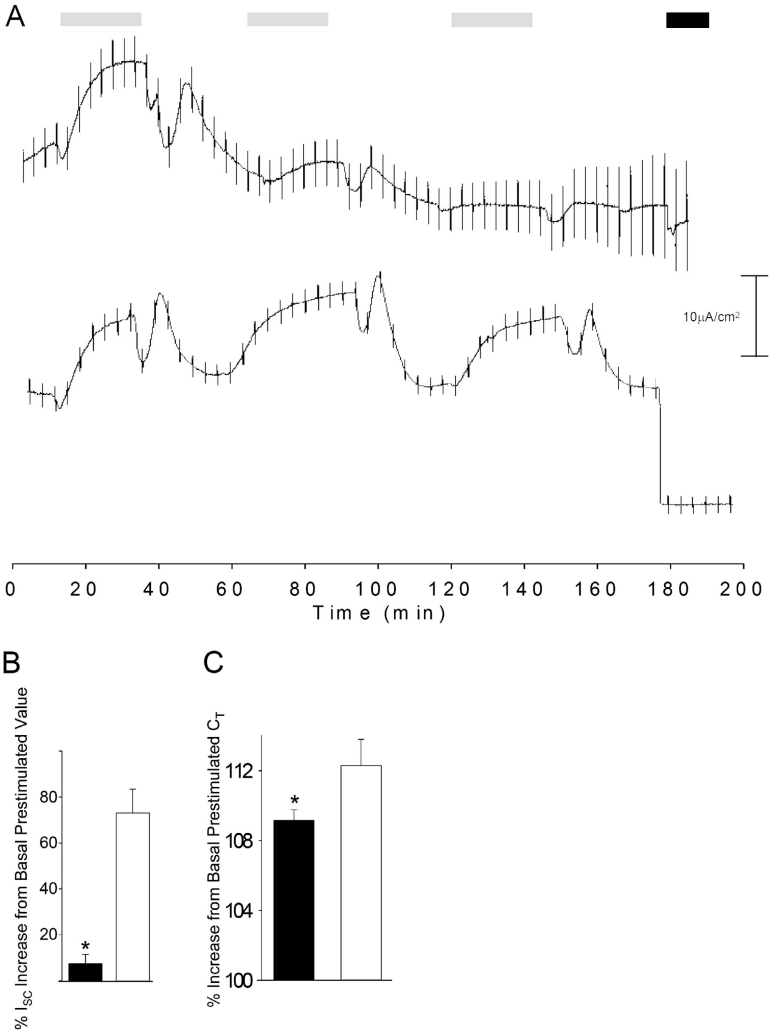

FIGURE 9. BFA treatment. (A) Representative trace demonstrating the effect of 5 μg/ml BFA on I_{SC} response (upper trace) to repetitive stimulations with the lower trace from control untreated epithelium from the same batch, age, and passage. (B) Summary of percentage I_{SC} increase a second forskolin stimulus elicited in BFA ($n = 8$) treated (black bar) compared with control (gray bar) epithelia ($n = 19$) demonstrated that the current response to forskolin was significantly smaller than control. (C) Percent C_T change for second forskolin stimulation in the presence of BFA ($n = 3$) (black bar) and control (gray bar) epithelia ($n = 15$; *, $P < 0.05$).

to nonselectively inhibit endocytic pathways by alkalinization of late endosomal vesicles (Tietze et al., 1980). CCD epithelia were preincubated in chloroquine for 4 h to elicit a maximal effect. Addition of chloroquine under basal conditions produced a steady increase in I_{SC} over 4 h (105 ± 45%, $n = 4$), presumably due to inhibition of channel endocytosis (see Fig. 10 C, below). Prolonged chloroquine incubation resulted in a reorganization of the endocytic compartment, as typical punctuate endosomal vesicles coalesced into larger structures (Fig. 10, A and B). The I_{SC} increase suggests that apical channel density under basal conditions is determined by a constitutive turnover of channels by endocytic and exocytic trafficking pathways.

During stimulation (Fig. 10 C), forskolin was able to elicit an initial response, but the increase in I_{SC} could not be reversed even with an extended wash protocol using double the wash volume. In addition, further ΔI_{SC} responses were attenuated due to the rising, poorly reversible current. These findings are summarized in Fig. 11 A, where the percent increase in I_{SC} for two successive forskolin stimulations is plotted. Therefore, the lack of response to a second forskolin stimulation probably reflects impaired channel retrieval from the apical surface. In addition, chloroquine prevented the reorganization of channels into a recycling pool following stimulus removal, since the capacitance response to a second stimulus was significantly reduced compared with control (Fig. 11 B). This, taken together with the fluorescence images (Fig. 10, A and B), indicates that chloroquine's effect may involve more than a collapse of pH gradients across endocytic vesicles; rather, it results in compartment rearrangement so that channels cannot be retrieved into the apical recycling pool.

Actin Is Required for ENaC Insertion, but not Retrieval

The trafficking of intracellular vesicles is closely associated with cytoskeletal elements (see reviews see Valentijn et al., 1999; Park et al., 2000; Eitzen, 2003). The effect of actin disruption on forskolin stimulation of ENaC currents was examined by selectively depolymerizing actin in CCD epithelia using LatA. The micro-

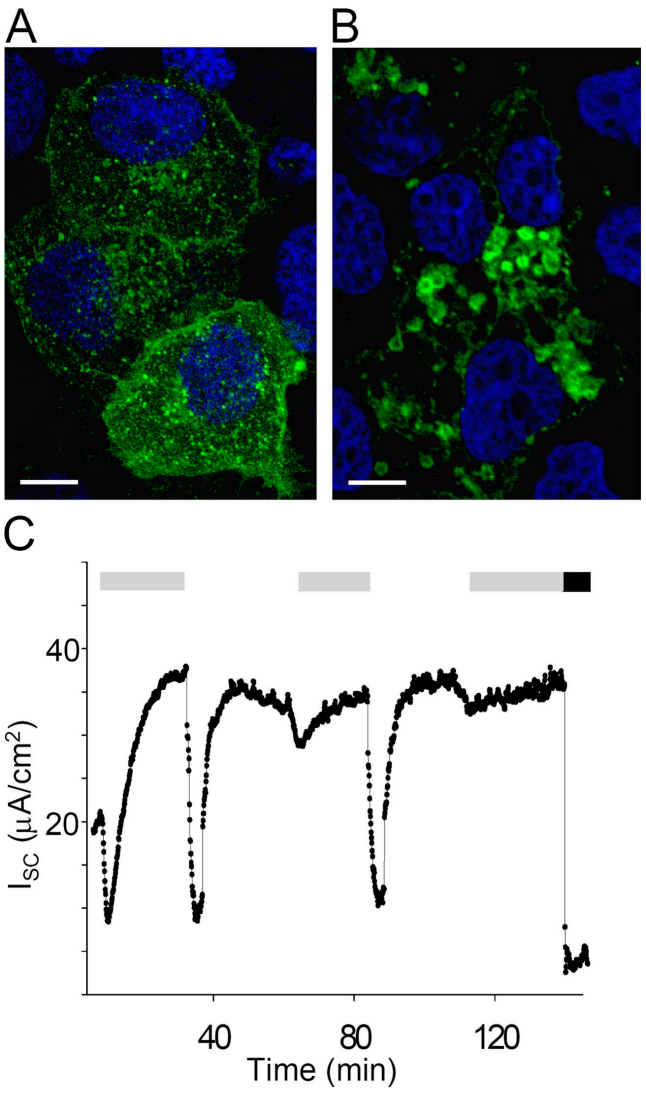

FIGURE 10. Chloroquine treatment. (A and B) Fluorescence micrographs from mCCD cells transiently expressing GFP-Endo to label endocytic compartments. Typical punctuate fluorescent staining pattern of endosomes (green) in untreated cells (A) collapsed to distended coalesced structures (B) in chloroquine-treated cells (white bar = 5 μm, nuclei labeled blue). (C) Representative I_{SC} trace from chloroquine-treated epithelium with repeated forskolin stimulation (gray bar). Note large dips in trace are the result of extended wash protocol to ensure total removal of forskolin from basal chamber. Addition of amiloride (black bar) following the third stimulation demonstrated that the majority of recorded I_{SC} was due to ENaC.

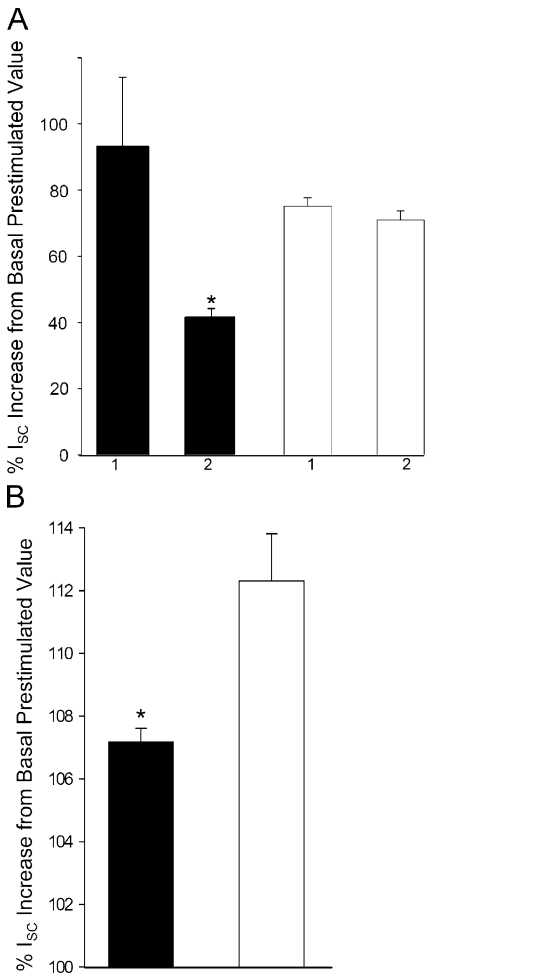

FIGURE 11. Chloroquine treatment summary. (A) Percentage I_{SC} increase for two forskolin stimulations (1 and 2). Control epithelia (white bar) produced ~80% increase in I_{SC} for each stimulation with the previously noted decline in response with successive stimuli. The first I_{SC} response for chloroquine-treated epithelia (black bar) was not statistically significantly different from control; however, ΔI_{SC} for the second stimulation was significantly reduced. (B) Percent C_T increase from prestimulated value for second forskolin stimulation (number 2 in A) indicates that chloroquine-treated cells (black bar) had a significantly reduced response when compared with controls ($n > 3$; *, $P < 0.05$).

graphs of Fig. 12 (A–C) illustrate actin disruption induced by a 30-min treatment with two concentrations of LatA, which induced depolymerization of actin stress fibers (at 200 nM) and a breakdown of cortical actin (at 1 μM). At 1 μM LatA, most intracellular actin was depolymerized, as reflected by the reduced phalloidin staining (Fig. 12 C). This breakdown of actin stress fibers was detected electrically as a reduction in transepithelial resistance or an increase in recorded conductance from 1.2 ± 0.2 mS before LatA treatment to 7.0 ± 0.4 mS ($n = 5$) at the end of the experiments. The point at which this occurred is evident from the current pulse magnitudes shown in Fig. 13 A. Nevertheless, it was possible to maintain the cells under voltage clamp for 30–60 min during the LatA-induced decline in R_T (from ~2,000 to ~200 Ω/cm²), but a prolonged restimulation protocol could not be performed. When LatA was added at the peak of the forskolin response (Fig. 13 A), it was possible to washout the agonist and return to the basal prestimulated I_{SC}; however, forskolin restimulation produced no significant I_{SC} response. Likewise, if LatA was added before forskolin stimu-

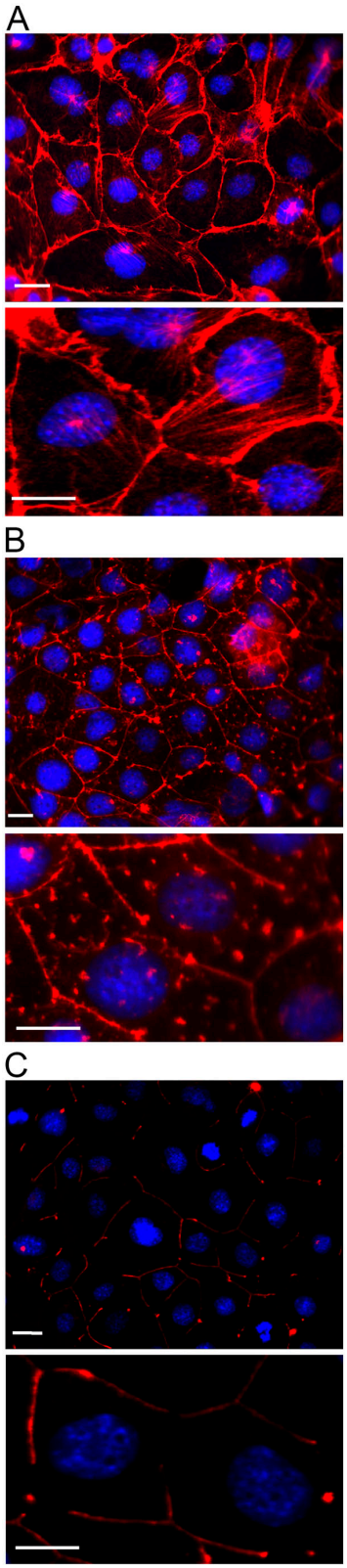

FIGURE 12. LatA. (A–C) Fluorescence micrographs of mCCD epithelia, phalloidin-labeled actin (red), and Hoechst-stained nuclei (blue). Untreated cells (A) exhibit typical cortical and filamentous actin staining that becomes progressively depolymerized with the addition of 200 nM (B) and 1 μM (C) LatA until most actin staining is lost. Areas of the micrographs are enlarged to show detail (white bar = 2 μm).

lation (Fig. 13 B), no significant ΔI_{SC} was observed. These findings suggest that actin is required to shuttle ENaC to the apical surface, but that it may not be critical for subsequent ENaC endocytosis. Fig. 13 C summarizes results from five experiments similar to the one presented in Fig. 13 A. The first forskolin I_{SC} response before LatA treatment is not significantly different from control cells. Following actin depolymerization, LatA-treated epithelia had a significantly reduced forskolin response when compared with control cells.

DISCUSSION

The mechanisms involved in the acute regulation of ENaC activity have been under investigation for some time in a number of model systems, such as toad urinary bladder (Coleman and Wade, 1994; Kleyman et al., 1994b; Weng and Wade, 1994), frog skin (Els et al., 1991; Lyall et al., 1994; Chou and Els, 1997; Nielsen, 1997), cultured A6 or M1 kidney cell lines (Marunaka and Eaton, 1991; Chalfant et al., 1993; Kleyman et al., 1994a; Verrey, 1994; Verrey et al., 1995; Edinger et al., 1999), and overexpression systems, and have employed a variety of physiological and biochemical methods (Reif et al., 1986; Garty and Palmer, 1997; Morris et al., 1998; Erlij et al., 1999; Weisz et al., 2000; Morris and Schafer, 2002; Rossier, 2002; Snyder, 2002). The cloning of ENaC (Canessa et al., 1994; McDonald et al., 1994, 1995) offered a new array of techniques, including antibody-based labeling; however, the mechanisms responsible for the acute regulation of ENaC activity at the apical surface have remained unclear.

Two hypotheses have been proposed to account for the acute increase in Na^+ transport that follows an intracellular cAMP rise, either a change in the open probability (P_o) of apical membrane-resident ENaC (Oh et al., 1993; Bradford et al., 1995; Senyk et al., 1995), possibly by direct channel phosphorylation (Shimkets et al., 1998), or the recruitment of ENaC from subapical storage pools to increase channel number (N) in the apical membrane (see Rossier, 2002; Snyder, 2002). These modes of regulation need not be mutually exclusive. Nevertheless, a body of evidence has accumulated to suggest that channels are recruited from intracellular stores and are inserted into the apical membrane on cAMP stimulation (Kleyman et al., 1994a; Snyder, 2000; Morris and Schafer, 2002). The subsequent fate of these channels (i.e., degradation versus recycling), as well as the source of channels entering the apically recruited pool (i.e., recycling versus synthesis), remains uncertain. By making use of repeti-

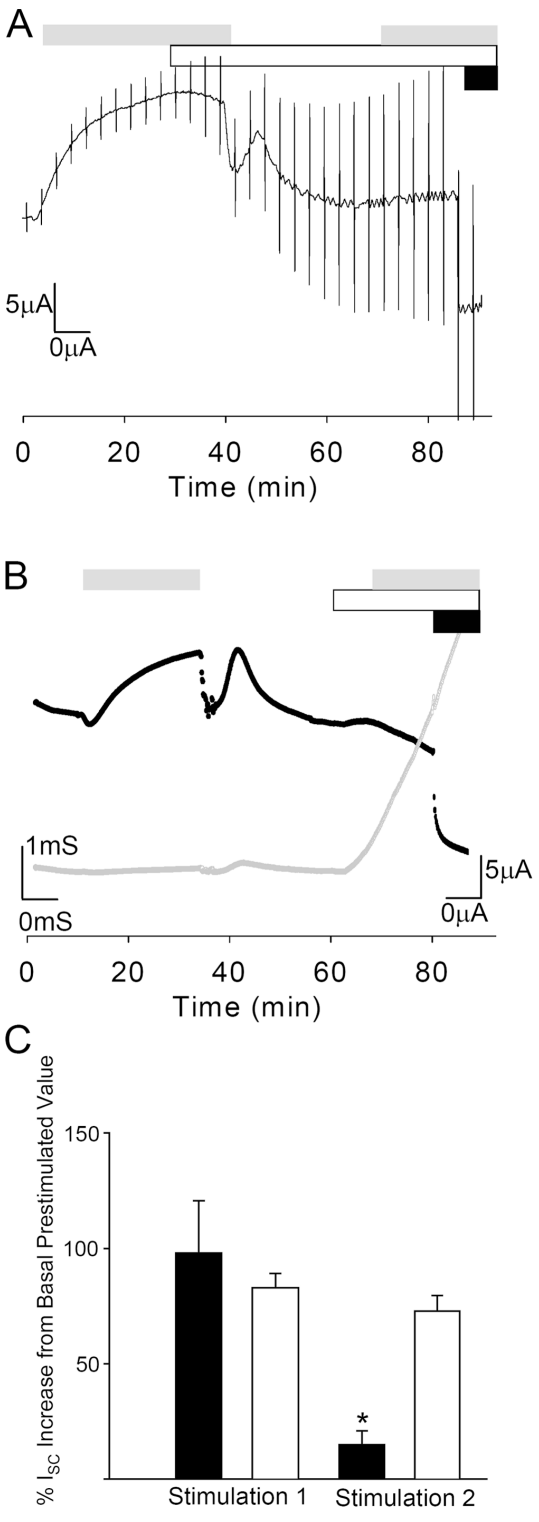

FIGURE 13. I_{SC} and G_T response to LatA. (A) Representative I_{SC} trace demonstrates that forskolin- induced I_{SC} stimulus (gray bar) returned to basal levels when LatA (white bar) was added at the peak of I_{SC} response. Readdition of forskolin did not elicit a subsequent stimulation (note that periodic voltage pulses increased on addition of LatA, indicating a loss in transepithelial resistance, but cells could be voltage clamped for the duration of the experiment). Addition of 10 μM amiloride (black bar) at the end of the trace indicated that the majority of the I_{SC} was I_{Na}. (B) Simultaneous I_{SC} (black trace) and G_T (gray trace) measurement demonstrated that the addition of LatA (white bar) after a round of forskolin stimulation and wash resulted in a loss in resistance (increase in conductance), but that the I_{SC} was not stimulated by addition of forskolin (gray bar). The calculated resistance at the end of the trace was ~200 Ω.cm² but cells could still be voltage clamped and current was inhibited by amiloride (as in A). (C) Summary of five similar experiments to A present forskolin I_{SC} responses to two rounds of stimulation (labeled 1 and 2) and indicate that LatA (black bars) significantly inhibited forskolin stimulation (second stimulation, 2) when compared with control epithelia (white bar).

tive cAMP stimulation of polarized mouse CCD epithelia, we have begun to address some of these issues. The data are consistent with the concept that much of the channel population that contributes to the cAMP-stimulated I_{Na} is inserted into the apical membrane from a recycling pool. In addition, a significant proportion of those channels retrieved from the apical surface following agonist washout are returned to this pool for further rounds of stimulation.

cAMP Stimulation Increases ENaC Number

The action of cAMP to increase apical ENaC number has been demonstrated previously using electrophysiological, biochemical, and imaging methods (Snyder, 2000; Butterworth et al., 2001; Morris and Schafer, 2002). These findings are further reinforced by the surface biotinylation data presented in Fig. 2. Densiometric quantitation of the Western blots demonstrated an increase in the three ENaC subunits exposed at the apical surface following forskolin stimulation. This apparent increase in channel number contributed an 83 ± 6% increase in I_{SC} and was paralleled by a 15.3 ± 1.5% increase in C_T. Forskolin stimulation was reversible, as I_{SC} and C_T declined to baseline levels on removal of the cAMP agonist; however, the potential for endocytosed ENaC to be organized into a recycling pool has not been investigated from a functional perspective. The targeting of ENaC for endocytic retrieval from the apical surface has been shown to involve the binding of Nedd4-2 WW domains with the PY motifs on ENaC COOH termini. This results in channel ubiquitination, endocytosis, and possible lysosome- and proteasome-mediated degradation (Goulet et al., 1998; Harvey et al., 1999; Abriel et al., 1999; Farr et al., 2000; Staub et al., 2000; Snyder et al., 2001, 2004; Debonneville and Staub, 2004). Nevertheless, we do not know how the extent of ENaC ubiquitination correlates with its endocytic retrieval and its eventual fate (i.e., degradation versus recycling).

Intracellular Source of ENaC for Apical Insertion

By repetitively stimulating CCD epithelia up to six times, it was possible to examine the influence of reagents that disrupt channel production or vesicle traf-

ficking on the cAMP-dependent ΔI_{SC}. Repeated stimulation produced a relatively small decline (~10%) in the forskolin response with each agonist addition, as shown in Fig. 4 B. Newly synthesized channels were not required to elicit these repetitive responses, since CHX preincubation produced a qualitatively similar response profile. ENaC production did, however, contribute to the recycling pool, as ΔI_{SC} declined at a faster rate than in control cells (~15%). In a study examining repeated vasopressin stimulation of toad urinary bladder, CHX treatment did not significantly alter the first response, but an ~20–30% decline in subsequent responses was noted (Weng and Wade, 1994).

Estimation of ENaC half-life using biochemical methods is one means of obtaining information about channel lifetimes under both basal and stimulated conditions. Nevertheless, previous studies have produced conflicting results, with half-lives ranging from minutes to several hours, depending on the methods and the system studied (Valentijn et al., 1998; Weisz et al., 2000; de la Rosa et al., 2002). In addition, differences have been reported in the half-lives of individual ENaC subunits. In a study investigating endogenously expressed channels in the A6 epithelia, de la Rosa et al. (2002) calculated a half-life of ~10–18 min for channels at the apical surface using a pulse-chase protocol, whereas the intracellular channel pool exhibited a half-life of 40–80 min. Differences in half-life may be due in part to the use of different cell lines or expression systems and experimental protocols performed at 22–28°C versus mammalian systems at 37°C. However, Weisz et al. (2000) made use of the same A6 cell line and demonstrated a long-lived (>24 h) half-life for the surface-labeled channel pool, whereas the half-life of the intracellular pool was shorter with the β-ENaC subunit half-life of only 5 h. These findings were in agreement with the observations of Kleyman et al. (2001), who found a long half-life for the αENaC subunits in A6 cells. Again in the same cell line, ^{35}S-methionine labeling of ENaC demonstrated a short (40–50 min) half-life for each ENaC subunit (May et al., 1997). In contrast, ENaC exogenously expressed in MDCK epithelia exhibited a half-life of ~60 min for both intracellular and surface ENaC (Hanwell et al., 2002). In oocytes, a half-life of ~4 h was obtained from pulse-chase experiments (Valentijn et al., 1998). A complication in these biochemical studies potentially arises from the use of various antibodies that may not recognize the recently identified furin-cleaved forms of channel subunits attributed to intracellular ENaC processing (Hughey et al., 2003, 2004a,b).

These findings could be consistent with either rapid channel degradation (apical $t_{1/2} \sim 15$ min) or with channel recycling (apical $t_{1/2}$ of several hours). A brief (min) apical ENaC half-life suggests that biosynthesis must be the predominant source of apically inserted channels, as most ENaC labeled at the surface would be degraded.

Nevertheless, these studies do not address the turnover of functional channels at the cell surface or their fate after endocytic retrieval. By examining ENaC currents in a polarized mammalian CCD cell line that endogenously expresses ENaC, we have collected data concerning the apical turnover of functional channels. Since currents remained fairly stable in the presence of CHX, including the ability to repeatedly stimulate I_{SC} with forskolin, our data suggests that active ENaC is fairly stable and longer lived than some previous biochemical studies suggest.

Contribution of Recycled Channels to Apical ENaC Insertion

The fairly persistent response to repeated stimulation could reflect a substantial intracellular storage pool of ENaC, rather than a channel recycling process. To further test the recycling hypothesis, $NiCl_2$ and benzamil was employed to selectively block ENaC at different times during repetitive stimulation. For $NiCl_2$ inhibition of the stimulated I_{SC}, a significant reduction in subsequent responses to forskolin suggested that channels irreversibly blocked by $NiCl_2$ were being returned to the membrane on restimulation. When channels were blocked by benzamil in the absence of agonist, the magnitude of the subsequent response to forskolin stimulation was not significantly different from that observed in untreated cells. This finding suggests that channels were inserted from a subapical pool that was not affected by benzamil block of channels at the epithelial surface.

When benzamil was added at the peak of the forskolin response, however, it was possible to elicit only small responses to restimulation ($\Delta I_{SC} = 12.5 \pm 2.6\%$ of control). This suggests that the majority of the channels that normally contribute to the restimulated I_{SC} response are retrieved from the apical surface after the prior stimulation. The small response to restimulation could result from dissociation of the slowly reversible blocker, or from channels delivered to the apical surface from another source, most likely the biosynthetic pathway. The results from CHX-treated cells suggest a ~5–10% contribution of channel biosynthesis to the observed ΔI_{SC} (Fig. 8), supporting this concept. Furthermore, benzamil did not affect the ΔC_T response to forskolin, suggesting that the trafficking mechanism that returns channels back to the apical membrane are independent of channel block.

Properties of the Recycling Pathway, Effects of BFA, Chloroquine, and LatA

We examined the actions on ENaC recycling of reagents that alter membrane trafficking and cytoskeletal organization using the restimulation protocol. Treatment with

BFA did not affect the first response to forskolin, but it produced a marked inhibition of the subsequent ΔI_{SC}. The finding that it was possible to elicit one cycle of forskolin stimulation–recovery suggests that ENaC-containing vesicles available for channel insertion are distal to the Golgi and TGN. The response to restimulation was significantly reduced, however, indicating that ENaC is recycled through BFA-sensitive compartments. Results from a study using BFA-treated toad bladder produced similar findings in response to repeated ADH stimulation; an initial stimulation could be elicited, but subsequent stimulations were abolished by pretreatment with 5 μg/ml BFA (Weng and Wade, 1994). The effect of BFA on ENaC recycling was unexpected in view of its well-documented inhibition of AP-1–dependent trafficking in early compartments of the protein secretory pathway. Endocytic retrieval of ENaC is anticipated to rely on AP-2–mediated processes, which are BFA insensitive, but this has not been demonstrated for ENaC. However, BFA has been observed to produce a tubulation of endosomal compartments (Lippincott-Schwartz et al., 1991; Prydz et al., 1992). It is also possible that reorganization of ENaC in the subapical pool involves trafficking through ARF-1/BFA-sensitive pathways.

The effect of disrupting the endocytic pathway with chloroquine was also examined. Chloroquine is reported to de-acidify endocytic compartments, preventing traffic of plasma membrane–derived vesicles to lysosomal and other degradation pathways (Tietze et al., 1980; Jones et al., 2004). If this were the only effect of chloroquine, a relatively slow accumulation of ENaC at the apical surface from biosynthetic pathways might be expected. A recycling channel population, when mobilized, would contribute to the accumulation of apical ENaCs. In agreement with these assumptions, the baseline ENaC current increased over time, with a maximum level reached at ~3–4 h (105 ± 45% increase over the initial current). It was possible to stimulate cells even at this elevated basal I_{SC}, but the stimulated currents could not be reversed, even by extensive washing. Studies of the cycling of Golgi proteins to the cell surface showed a chloroquine-induced redistribution of early endosomal markers into enlarged vesicles lacking compartment identity (Puri et al., 2002). Although these cells were not labeled with early endocytic compartment reporters, it is reasonable to assume from previous work that they would be redistributed into these enlarged structures (Linstedt et al., 1997; Bachert et al., 2001). Similarly, it is likely that essential endocytic trafficking proteins accumulate within these structures and are therefore not available for channel retrieval and redistribution. This disruption of the recycling compartment, together with the accumulation of ENaC at the cell surface, disturbed the normal membrane trafficking response to restimulation, which was reflected by a reduction in the forskolin-induced C_T response.

The extent of actin cytoskeletal involvement in ENaC recycling was assessed by selectively depolymerizing F-actin in mCCD epithelia using LatA. Addition of LatA before forskolin diminished the I_{SC} stimulation observed in control cells. A significantly reduced I_{SC} response to forskolin addition was observed for all investigations of LatA-treated cells (all recordings were longer than 15 min after forskolin addition). In contrast, LatA treatment did not affect recovery from forskolin stimulation washout. These results indicate that an intact actin cytoskeleton is required for ENaC insertion, but is not required for subsequent channel endocytosis. This finding agrees with previous studies in frog skin that examined the effect of actin depolymerization on the response to vasopressin (Els and Chou, 1993). Other studies have implicated a direct actin/ENaC interaction in the modulation of channel gating and conductance, with different forms of actin added to ENaC reconstituted in lipid bilayers or coexpressed in oocytes (Jovov et al., 1999; Berdiev et al., 2001; Copeland et al., 2001). The addition of LatA either before or at the peak of the forskolin response did not alter steady-state ENaC currents, even when it was clear from the drop in transepithelial resistance that LatA had elicited actin depolymerization. We cannot, however, preclude the association of actin with ENaC in the membrane, even though apical actin staining was largely abolished.

ENaC Recycling Model

The concept that ENaC is acutely inserted into the apical membrane of Na^+-absorbing epithelia from a vesicle-based recycling pool is supported by several results emerging from the repetitive stimulation protocol described here. A model to describe ENaC insertion–recycling pathways was developed using software (Model Maker V4; Model Kinetix) to fit the time courses of I_{SC} responses in control experiments, and these compartments and kinetic parameters were then tested using results from experiments where ENaC trafficking was perturbed. A schematic of the rates and corresponding half-lives included in the model under control conditions is presented in Fig. 14.

The apical membrane was described as a compartment where channels were inserted or retrieved according to rates obtained from the control data. Stimulation or retrieval events were set to occur at 30-min intervals, to match the timing of forskolin stimulation and washout periods; no attempt was made to model the transient in I_{SC} observed when the basolateral chambers were washed. A value of 100 (channels) was arbitrarily assigned to the apical compartment; also, no alteration in P_o or unitary current during these responses was assumed, so that the derived I_{SC} trace re-

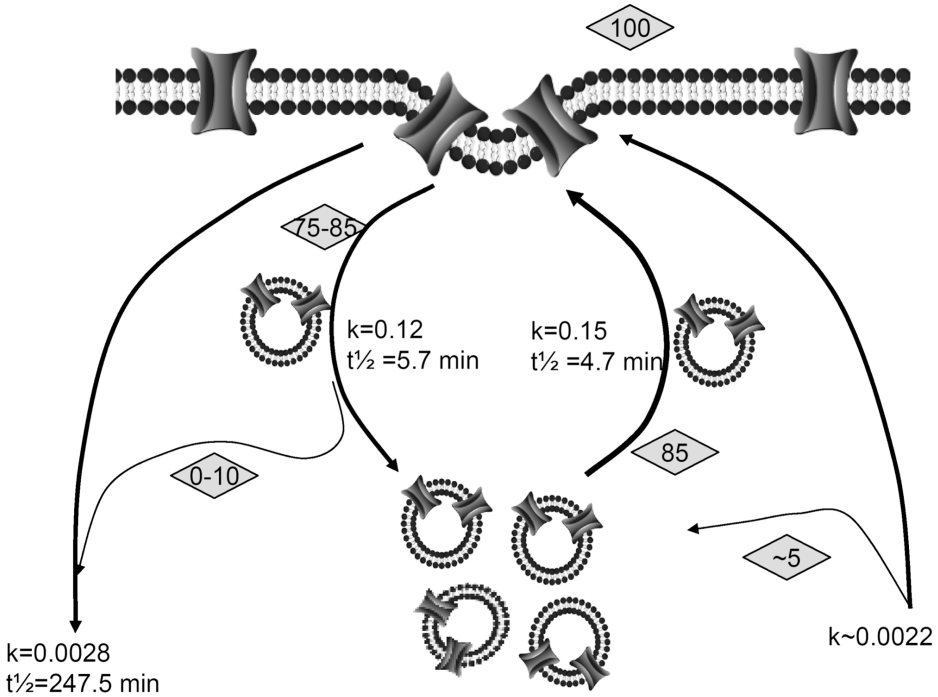

FIGURE 14. Schematic model of ENaC recycling pathways. Rates (k) and $t_{1/2}$ values as calculated from I_{SC} measurements are provided for each pathway, and were used to model the recycling kinetics as described in the text (see Fig. 15). Values in shaded diamonds represent the relative pool sizes (percent of basal I_{SC}, i.e., number of functional channels) derived from these pathways.

flects only percent changes in channel number at the cell surface.

The repetitive stimulation protocol under control conditions was modeled with the assumption that ENaC is derived entirely from the intracellular recycling pool. Since the average maximum I_{SC} response was 83 ± 6%, the size of the recycling pool was set to an initial value of 85. ENaC insertion was modeled as a single exponential rise to a maximum value, using insertion rate constants calculated from the control data. Recovery from stimulation was modeled as an exponential decay, again using rates calculated from the control data. In the model, all channels retrieved during a 30-min washout were placed back into the recycling compartment (less those lost to degradation or not endocytosed), to be available for insertion on the next stimulation. The rate of current decay measured in the presence of CHX in unstimulated epithelia was used to define the biosynthetic production rate of functional channels, and this, together with a degradation component, was included in the model to account for channel turnover. From these data, it was not possible to detect the presence of multiple series compartments, e.g., within the recycling pathway; therefore, the model was constructed with only two compartments, the apical membrane and the recycling pool.

Once a single control trace was obtained, channel insertion and/or retrieval rates were altered to simulate the experimental results (Fig. 15). The simulated trace illustrating changes in functional channel number with repeated stimulation over time is presented in Fig. 15 A (trace 1). The model approximates real data, but with some observable differences. First, the rate of channel insertion with each stimulation declined in the actual recordings, but this was not recapitulated in the model, since subsequent responses were initially modeled with identical parameters to that of the first. Second, the decline in ΔI_{SC} with time can be attributed to a failure of channels to reenter the recycling pool during recovery, either due to insufficient time between stimuli or to degradative loss. However, the loss in ΔI_{SC} in actual traces was more rapid than predicted by the model. When a loss of 2–5% of the recycling channels was included in each round of stimulation, the model approximated the actual data with reasonable accuracy (Fig. 15 A, trace 1 vs. 2). Having achieved a reasonable simulation of the control I_{SC} traces, model parameters were altered to predict changes in cell surface ENaC number following perturbations in channel production or trafficking.

To simulate CHX block of ENaC synthesis, the channel production rate was set to zero. The resulting traces approximated the data closely (Fig. 15 B), with the drop in I_{SC} due primarily to a decline in apical insertion rate. After the fourth stimulus, there was no additional response to stimulation, as the supply of channels entering the recycling pool was exhausted. Thus, although the contribution of ENaC synthesis to individual I_{SC} responses is minor relative to the recycling pathway, it becomes highly significant when there is multiple repetitive turnover of the apical pool. It was not possible to determine whether newly synthesized channels are destined primarily for the apical membrane or the recycling compartment, and additional experiments to target these pathways will be required.

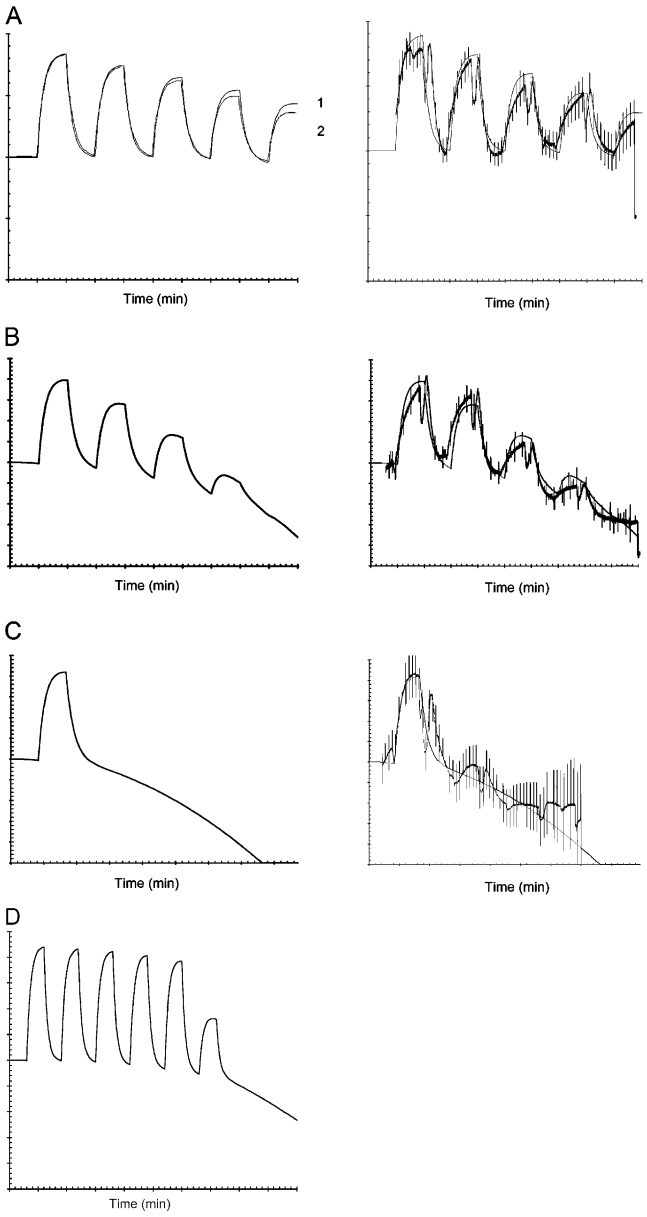

FIGURE 15. Model I_{SC} predictions. (A) Trace 1 produced using measured I_{SC} kinetics (see Fig. 14 for values) presented on the left panel. The model was altered to account for channel loss from the recycling pool (see text) and produced a more rapid ΔI_{SC} decline (trace 2), which better fit experimental recordings (right panel shows actual trace overlaid with curve 2 from modeled data). (B) The I_{SC} trace describing CHX treatment (left) was obtained by blocking the production pathway on the model, which closely approximated actual recordings (right panel). (C) BFA treatment was modeled as a single stimulation event after which no additional channel insertion event was permitted (left) to simulate block of ENaC delivery to the cell surface. Actual I_{SC} recordings overlaid on the model trace (right) show that some channel delivery still occurred following BFA treatment. (D) Trace from an alternative model, which includes a large intracellular channel pool. ENaC does not return to this pool following agonist washout. The predicted I_{SC} trace does not resemble actual data from control epithelia (as in A) since ΔI_{SC} does not decline significantly with repetitive stimulations until the channel store is exhausted.

To model the action of BFA, which is reported to inhibit anterograde trafficking from the TGN, the recycling channel pool was kept intact, consistent with the initial stimulation–recovery cycle that was unperturbed in BFA-treated cells. Thereafter, ENaC trafficking to the surface membrane was prevented by setting subsequent insertion rates (from both recycling and synthesis) to zero. As expected, the model produced only one response (Fig. 15 C), followed by decay of the basal current. The model accounted for the current decay due to block of synthetic delivery (as for CHX), but the presence of small subsequent responses in the actual experimental data indicates that BFA did not completely block channel insertion. Either the action of BFA was incomplete, or a model featuring insertion of only a fraction of channels in the recycling pool would provide a better description of the data. In the latter case, multiple series compartments within the recycling pathway may provide a more realistic scheme.

The concept of a channel recycling pool is supported by this compartmental model. Other hypotheses were tested but failed to generate simulations that approximated the data as well as the model of Fig. 14, but one in particular deserves comment. The concept of a large subapical pool of channels that does not reload from the apical compartment could contribute to repetitive responses; in this model, retrieved channels were targeted directly to the degradation pathway. The I_{SC} trace predicted for this model (Fig. 15 D) shows that the forskolin response remains fairly consistent until the intracellular channel pool (set at 500) is exhausted, at which time the current responses are eliminated. The abrupt drop in ΔI_{SC} predicted by this model was not observed. Although the timing of current collapse would be determined by the initial pool size, the consistency of individual responses (lack of ΔI_{SC} decay) does not recapitulate observed traces (Fig. 15 A). Thus, although there appear to be large pools of individual channel subunits intracellularly in some systems, especially in studies where ENaC is overexpressed (Valentijn et al., 1998), a model featuring recruitment from such a pool without channel recycling does not provide the best description of these data.

Conclusions

By examining the I_{SC} and C_T responses to repetitive cAMP stimulation of mouse CCD epithelia, a subapical channel ENaC recycling pool has been identified. ENaC is recruited to the apical membrane from this pool on acute stimulation, and following stimulus removal, a large fraction of the endocytosed channels is returned to this recycling compartment, to be available for additional agonist responses. A simple compartmental model provides theoretical support for the presence of this ENaC recycling pool. Definition of the

number and nature of the intracellular compartments comprising the ENaC recycling pathway will require additional studies.

APPENDIX

Nyquist Plots

The epithelium was modeled in the usual manner (Fig. A1), as an equivalent circuit consisting of serial RC elements corresponding to the apical and basolateral membranes, together with the parallel, paracellular resistance. The epithelial impedance is displayed as a Nyquist plot, permitting calculation of the total epithelial capacitance. The latter is determined by the area of the individual membranes (typically 1 $\mu F/cm^2$) and its dielectric properties. The transepithelial impedance (Z_T) of membranes in such a model has been described previously (Paunescu and Helman, 2001a) as

$$Z_T = \frac{(Z_a + Z_b)R_p}{Z_a + Z_b + R_p},$$

where R_p is the paracellular (shunt) resistance (see model circuit) and Z_a and Z_b are the impedances of the apical and basolateral membranes, respectively. By examining current response to an imposed sinusoidal voltage, the impedance of a single membrane (Z_m) at a given frequency can be described as (Singh et al., 2002)

$$Z_m(f) = \frac{R_m}{1 + (R_m C_m j\omega)^{\alpha}},$$

where $j = \sqrt{-1}$, $\alpha = 2\phi/\pi$, and ϕ = phase shift angle in degrees.

It was demonstrated previously that the measured capacitance is frequency dependent (Paunescu and Helman, 2001a), especially at lower frequencies, making the time constants for the RC element frequency dependent. This was verified using the present experimental system (Van Driessche et al., 1999), which records epithelial capacitance values at five frequencies simultaneously. However, all values for capacitance were obtained >4 kHz where C_T values become independent of the membrane resistance, as noted above. According to the model below, C_T is determined by the capacitances of the apical and basal membrane in series:

$$\frac{1}{C_T} = \frac{1}{C_a} + \frac{1}{C_b}.$$

As the calculation of Z_m yields a complex number, the results are presented as a Nyquist plot, in which the magnitude and phase of the frequency response are plotted on orthogonal axes, real and imaginary. Points are plotted for each frequency in a logarithmic range of 78 frequencies in this application.

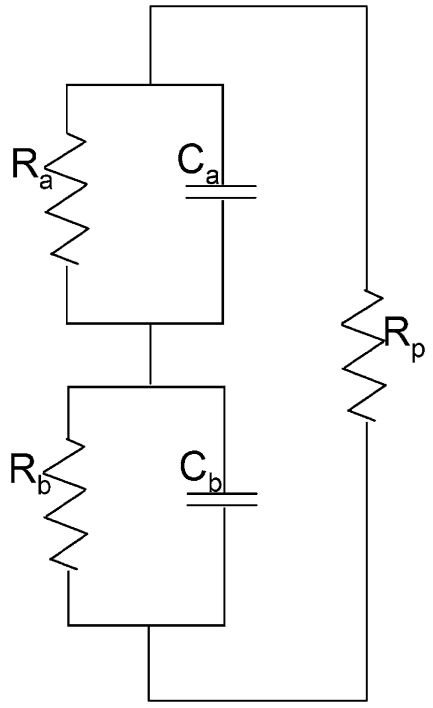

FIGURE A1. Model RC circuit. A schematic representation of the simple model circuit that represents a polarized epithelium used to calculate capacitance. Apical and basal membranes are described as a parallel resistor (R_a and R_b) and capacitor (C_a and C_b) connected in series. The paracellular resistance (R_p) is connected in parallel.

Compartmental Modeling

The modeled traces were obtained by making use of object modeling software (Model Maker V4; Model Kinetix), which readily allowed schematic compartmental models to be constructed. The model was integrated over desired time courses to produce a model trace. The recycling pool (described in DISCUSSION) and apical membrane were constructed as compartments as illustrated in Fig. A2. Rates of insertion and retrieval for acute and constitutive ENaC trafficking were calculated from recorded amiloride-sensitive I_{SC} responses to forskolin and forskolin washout and CHX treatments, respectively. Insertion and retrieval events were modeled as single exponential rise and decays for each compartment; for example, for the first round of stimulation, channels inserted into the apical membrane from the recycling pool could be described by

$$M_t = M_0 + R \cdot (1 - e^{-k_i t}), \quad \text{(A1)}$$

where $M_0 = 100$ (starting value), $R = 85$, and $k_i = 0.15$ min^{-1}.

For the first stimulus washout event, removal of channels from the apical surface to the recycling compartment would be described by

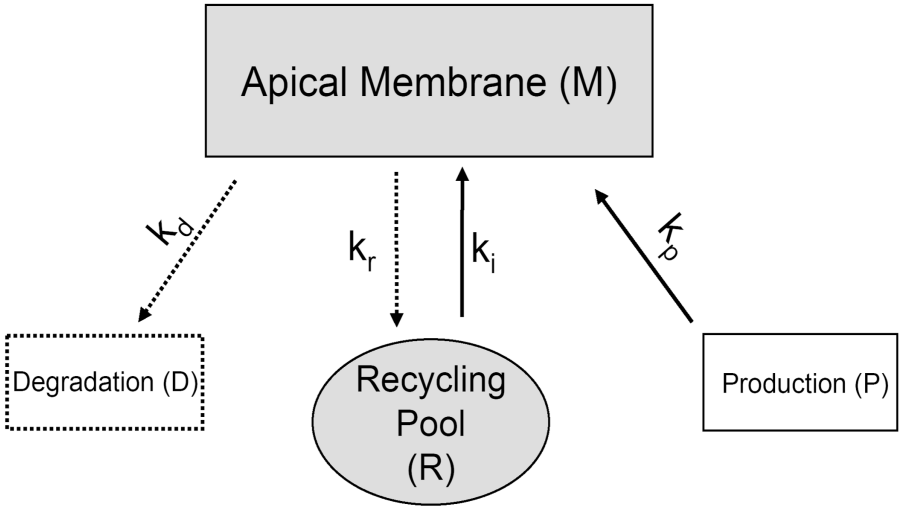

FIGURE A2. Schematic compartmental model. The arrangement of intracellular channel recycling pool and apical membrane used for modeling repetitive forskolin stimulations is presented in the schematic compartmental model. Associated rates for movement of channels between compartments is presented adjacent to arrows connecting compartments and these were used in equations described in the text to model trafficking events.

$$M_t = M_{30} - M \cdot e^{-k_r t}, \quad \text{(A2)}$$

where M_{30} = value of membrane channel pool at start of retrieval event = prestimulated value + inserted channels and $k_r = 0.14\ min^{-1}$.

Thus, the rate of change of the apical membrane channel pool during insertion events, set to occur over 30 min, was described as insertion from the recycling pool and production, with constitutive degradation by the following differential equation:

$$\frac{dMt}{dt} = -k_d(M) + k_i(R) + k_p(P), \quad \text{(A3)}$$

with M = 100, R = 85, P = 10,000 (initial values), $k_i = 0.15\ min^{-1}$, $k_p = 0.0022\ min^{-1}$, $k_d = 0.0028\ min^{-1}$.

Rates of the stimulus-washout events were set to start after a 30-min insertion event and were described as removal from the apical membrane (retrieval) and loss to degradation with constitutive insertion from production as

$$\frac{dMt}{dt} = +k_p(P) - (k_r + k_d)(M), \quad \text{(A4)}$$

with $M = M_0$ + number of inserted channels (e.g., after 30 min $M_{30} = 183$) and $k_r = 0.14\ min^{-1}$.

The authors would like to thank C. Rice and C. King for technical assistance and Drs. Kathryn Peters and Mark Knepper for donation of ENaC antibodies.

This work is supported by the National Institutes of Health grants RO1 DK54814 (to R.A. Frizzell) and R01 DK057718 (to J.P. Johnson) and by a postdoctoral fellowship from the Cystic Fibrosis Foundation and training grant DK061296-03 (M.B. Butterworth).

Lawrence G. Palmer served as editor.

Submitted: 10 June 2004
Accepted: 7 December 2004

REFERENCES

Abriel, H., J. Loffing, J.F. Rebhun, J.H. Pratt, L. Schild, J.D. Horisberger, D. Rotin, and O. Staub. 1999. Defective regulation of the epithelial Na^+ channel by Nedd4 in Liddle's syndrome. *J. Clin. Invest.* 103:667–673.

Bachert, C., T.H. Lee, and A.D. Linstedt. 2001. Lumenal endosomal and Golgi-retrieval determinants involved in pH-sensitive targeting of an early Golgi protein. *Mol. Biol. Cell.* 12:3152–3160.

Benos, D.J., M.S. Awayda, I.I. Ismailov, and J.P. Johnson. 1995. Structure and function of amiloride-sensitive Na^+ channels. *J. Membr. Biol.* 143:1–18.

Berdiev, B.K., R. Latorre, D.J. Benos, and I.I. Ismailov. 2001. Actin modifies Ca^{2+} block of epithelial Na^+ channels in planar lipid bilayers. *Biophys. J.* 80:2176–2186.

Bradford, A.L., I.I. Ismailov, J.M. Achard, D.G. Warnock, J.K. Bubien, and D.J. Benos. 1995. Immunopurification and functional reconstitution of a Na^+ channel complex from rat lymphocytes. *Am. J. Physiol.* 269:C601–C611.

Butterworth, M.B., S.I. Helman, and W.J. Els. 2001. cAMP-sensitive endocytic trafficking in A6 epithelia. *Am. J. Physiol. Cell Physiol.* 280:C752–C762.

Canessa, C.M., L. Schild, G. Buell, B. Thorens, I. Gautschi, J.D. Horisberger, and B.C. Rossier. 1994. Amiloride-sensitive epithelial Na^+ channel is made of three homologous subunits. *Nature.* 367:463–467.

Chalfant, M.L., B. Coupaye-Gerard, and T.R. Kleyman. 1993. Distinct regulation of Na^+ reabsorption and Cl^- secretion by arginine vasopressin in the amphibian cell line A6. *Am. J. Physiol.* 264: C1480–C1488.

Chou, K.Y., and W.J. Els. 1997. Effects of disassembly of actin microfilaments on the AVP-induced regulation of sodium channel densities in frog skin epithelium. *Biol. Cell.* 89:285–294.

Coleman, R.A., and J.B. Wade. 1994. ADH-induced recycling of fluid-phase marker from endosomes to the mucosal surface in toad bladder. *Am. J. Physiol.* 267:C32–C38.

Copeland, S.J., B.K. Berdiev, H.L. Ji, J. Lockhart, S. Parker, C.M. Fuller, and D.J. Benos. 2001. Regions in the carboxy terminus of α-bENaC involved in gating and functional effects of actin. *Am. J. Physiol. Cell Physiol.* 281:C231–C240.

de la Rosa, D.A., H. Li, and C.M. Canessa. 2002. Effects of aldosterone on biosynthesis, traffic, and functional expression of epithelial sodium channels in A6 cells. *J. Gen. Physiol.* 119:427–442.

Debonneville, C., and O. Staub. 2004. Participation of the ubiquitin-conjugating enzyme UBE2E3 in Nedd4-2-dependent regu-

lation of the epithelial Na^+ channel. *Mol. Cell. Biol.* 24:2397–2409.

Dikic, I. 2003. Mechanisms controlling EGF receptor endocytosis and degradation. *Biochem. Soc. Trans.* 31:1178–1181.

Ecelbarger, C.A., G.H. Kim, J.B. Wade, and M.A. Knepper. 2001. Regulation of the abundance of renal sodium transporters and channels by vasopressin. *Exp. Neurol.* 171:227–234.

Edinger, R.S., M.D. Rokaw, and J.P. Johnson. 1999. Vasopressin stimulates sodium transport in A6 cells via a phosphatidylinositide 3-kinase-dependent pathway. *Am. J. Physiol.* 277:F575–F579.

Eitzen, G. 2003. Actin remodeling to facilitate membrane fusion. *Biochim. Biophys. Acta.* 1641:175–181.

Els, W.J., and M.B. Butterworth. 1998. Cytochemical localization of adenylate cyclase in cultured renal epithelial (A6) cells. *Microsc. Res. Tech.* 40:455–462.

Els, W.J., and K.Y. Chou. 1993. Sodium-dependent regulation of epithelial sodium channel densities in frog skin; a role for the cytoskeleton. *J. Physiol.* 462:447–464.

Els, W.J., S.I. Helman, and T. Mencio. 1991. Activation of epithelial Na channels by hormonal and autoregulatory mechanisms of action. *J. Gen. Physiol.* 98:1197–1220.

Erlij, D., P. De Smet, D. Mesotten, and W. Van Driessche. 1999. Forskolin increases apical sodium conductance in cultured toad kidney cells (A6) by stimulating membrane insertion. *Pflugers Arch.* 438:195–204.

Erlij, D., P. De Smet, and W. Van Driessche. 1994. Effect of insulin on area and Na^+ channel density of apical membrane of cultured toad kidney cells. *J. Physiol.* 481(Pt 3):533–542.

Farr, T.J., S.J. Coddington-Lawson, P.M. Snyder, and F.J. McDonald. 2000. Human Nedd4 interacts with the human epithelial Na^+ channel: WW3 but not WW1 binds to Na^+-channel subunits. *Biochem. J.* 345(Pt 3):503–509.

Firsov, D., I. Gautschi, A.M. Merillat, B.C. Rossier, and L. Schild. 1998. The heterotetrameric architecture of the epithelial sodium channel (ENaC). *EMBO J.* 17:344–352.

Firsov, D., L. Schild, I. Gautschi, A.M. Merillat, E. Schneeberger, and B.C. Rossier. 1996. Cell surface expression of the epithelial Na channel and a mutant causing Liddle syndrome: a quantitative approach. *Proc. Natl. Acad. Sci. USA.* 93:15370–15375.

Fujii, Y., and A.I. Katz. 1989. Direct Na^+-K^+ pump stimulation by K^+ in cortical collecting tubules: a mechanism for early renal K^+ adaptation. *Am. J. Physiol.* 257:F595–F601.

Garty, H., and L.G. Palmer. 1997. Epithelial sodium channels: function, structure, and regulation. *Physiol. Rev.* 77:359–396.

Gormley, K., Y. Dong, and G.A. Sagnella. 2003. Regulation of the epithelial sodium channel by accessory proteins. *Biochem. J.* 371: 1–14.

Goulet, C.C., K.A. Volk, C.M. Adams, L.S. Prince, J.B. Stokes, and P.M. Snyder. 1998. Inhibition of the epithelial Na^+ channel by interaction of Nedd4 with a PY motif deleted in Liddle's syndrome. *J. Biol. Chem.* 273:30012–30017.

Hanukoglu, A. 1991. Type I pseudohypoaldosteronism includes two clinically and genetically distinct entities with either renal or multiple target organ defects. *J. Clin. Endocrinol. Metab.* 73:936–944.

Hanwell, D., T. Ishikawa, R. Saleki, and D. Rotin. 2002. Trafficking and cell surface stability of the epithelial Na^+ channel expressed in epithelial Madin-Darby canine kidney cells. *J. Biol. Chem.* 277: 9772–9779.

Harvey, K.F., A. Dinudom, P. Komwatana, C.N. Jolliffe, M.L. Day, G. Parasivam, D.I. Cook, and S. Kumar. 1999. All three WW domains of murine Nedd4 are involved in the regulation of epithelial sodium channels by intracellular Na^+. *J. Biol. Chem.* 274:12525–12530.

Hughey, R.P., J.B. Bruns, C.L. Kinlough, K.L. Harkleroad, Q. Tong, M.D. Carattino, J.P. Johnson, J.D. Stockand, and T.R. Kleyman. 2004a. Epithelial sodium channels are activated by furin-dependent proteolysis. *J. Biol. Chem.* 279:18111–18114.

Hughey, R.P., J.B. Bruns, C.L. Kinlough, and T.R. Kleyman. 2004b. Distinct pools of epithelial sodium channels are expressed at the plasma membrane. *J. Biol. Chem.* 279:48491–48494.

Hughey, R.P., G.M. Mueller, J.B. Bruns, C.L. Kinlough, P.A. Poland, K.L. Harkleroad, M.D. Carattino, and T.R. Kleyman. 2003. Maturation of the epithelial Na^+ channel involves proteolytic processing of the α- and γ-subunits. *J. Biol. Chem.* 278:37073–37082.

Ito, Y., H. Kume, K. Yamaki, and K. Takagi. 1999. Tetracyclines reduce Na^+/K^+ pump capacity in Calu-3 human airway cells. *Biochem. Biophys. Res. Commun.* 260:13–16.

Jones, H.M., K.L. Hamilton, G.D. Papworth, C.A. Syme, S.C. Watkins, N.A. Bradbury, and D.C. Devor. 2004. Role of the NH2 terminus in the assembly and trafficking of the intermediate conductance Ca^{2+}-activated K^+ channel hIK1. *J. Biol. Chem.* 279: 15531–15540.

Jovov, B., A. Tousson, H.L. Ji, D. Keeton, V. Shlyonsky, P.J. Ripoll, C.M. Fuller, and D.J. Benos. 1999. Regulation of epithelial Na^+ channels by actin in planar lipid bilayers and in the *Xenopus* oocyte expression system. *J. Biol. Chem.* 274:37845–37854.

Kellenberger, S., I. Gautschi, and L. Schild. 2003. Mutations in the epithelial Na^+ channel ENaC outer pore disrupt amiloride block by increasing its dissociation rate. *Mol. Pharmacol.* 64:848–856.

Kellenberger, S., and L. Schild. 2002. Epithelial sodium channel/degenerin family of ion channels: a variety of functions for a shared structure. *Physiol. Rev.* 82:735–767.

Kleyman, T.R., T. Yulo, C. Ashbaugh, D. Landry, E.J. Cragoe, A. Karlin, and Q. Al Awqati. 1986. Photoaffinity labeling of the epithelial sodium channel. *J. Biol. Chem.* 261:2839–2843.

Kleyman, T.R., S.A. Ernst, and B. Coupaye-Gerard. 1994a. Arginine vasopressin and forskolin regulate apical cell surface expression of epithelial Na^+ channels in A6 cells. *Am. J. Physiol.* 266:F506–F511.

Kleyman, T.R., P.R. Smith, and D.J. Benos. 1994b. Characterization and localization of epithelial Na^+ channels in toad urinary bladder. *Am. J. Physiol.* 266:C1105–C1111.

Kleyman, T.R., J.B. Zuckerman, P. Middleton, K.A. McNulty, B. Hu, X. Su, B. An, D.C. Eaton, and P.R. Smith. 2001. Cell surface expression and turnover of the alpha-subunit of the epithelial sodium channel. *Am. J. Physiol.* 281:F213–F221.

Liddle, G.W., T. Bledsoe, and W.S. Coppage. 1963. A familial renal disorder simulating primary aldosteronism but with negligible aldosterone secretion. *Trans. Assoc. Am. Physicians.* 76:199–213.

Linstedt, A.D., A. Mehta, J. Suhan, H. Reggio, and H.P. Hauri. 1997. Sequence and overexpression of GPP130/GIMPc: evidence for saturable pH-sensitive targeting of a type II early Golgi membrane protein. *Mol. Biol. Cell.* 8:1073–1087.

Lippincott-Schwartz, J., L. Yuan, C. Tipper, M. Amherdt, L. Orci, and R.D. Klausner. 1991. Brefeldin A's effects on endosomes, lysosomes, and the TGN suggest a general mechanism for regulating organelle structure and membrane traffic. *Cell.* 67:601–616.

Lyall, V., T.S. Belcher, J.H. Miller, and T.U. Biber. 1994. Na^+ transport and pH in principal cells of frog skin: effect of antidiuretic hormone. *Am. J. Physiol.* 267:R107–R114.

Malik, B., L. Schlanger, O. Al Khalili, H.F. Bao, G. Yue, S.R. Price, W.E. Mitch, and D.C. Eaton. 2001. ENaC degradation in A6 cells by the ubiquitin-proteosome proteolytic pathway. *J. Biol. Chem.* 276:12903–12910.

Mall, M., B.R. Grubb, J.R. Harkema, W.K. O'Neal, and R.C. Boucher. 2004. Increased airway epithelial Na^+ absorption produces cystic fibrosis-like lung disease in mice. *Nat. Med.* 10:487–493.

Marunaka, Y., and D.C. Eaton. 1991. Effects of vasopressin and cAMP on single amiloride-blockable Na channels. *Am. J. Physiol.* 260:C1071–C1084.

May, A., A. Puoti, H.P. Gaeggeler, J.D. Horisberger, and B.C. Rossier. 1997. Early effect of aldosterone on the rate of synthesis of the epithelial sodium channel α subunit in A6 renal cells. *J. Am. Soc. Nephrol.* 8:1813–1822.

McDonald, F.J., M.P. Price, P.M. Snyder, and M.J. Welsh. 1995. Cloning and expression of the β- and γ-subunits of the human epithelial sodium channel. *Am. J. Physiol.* 268:C1157–C1163.

McDonald, F.J., P.M. Snyder, P.B. McCray Jr., and M.J. Welsh. 1994. Cloning, expression, and tissue distribution of a human amiloride-sensitive Na^+ channel. *Am. J. Physiol.* 266:L728–L734.

Morris, R.G., and J.A. Schafer. 2002. cAMP increases density of ENaC subunits in the apical membrane of MDCK cells in direct proportion to amiloride-sensitive Na^+ transport. *J. Gen. Physiol.* 120:71–85.

Morris, R.G., A. Tousson, D.J. Benos, and J.A. Schafer. 1998. Microtubule disruption inhibits AVT-stimulated Cl^- secretion but not Na^+ reabsorption in A6 cells. *Am. J. Physiol.* 274:F300–F314.

Nielsen, R. 1997. Correlation between transepithelial Na^+ transport and transepithelial water movement across isolated frog skin (*Rana esculenta*). *J. Membr. Biol.* 159:61–69.

Oh, Y., P.R. Smith, A.L. Bradford, D. Keeton, and D.J. Benos. 1993. Regulation by phosphorylation of purified epithelial Na^+ channels in planar lipid bilayers. *Am. J. Physiol.* 265:C85–C91.

Palmer, L.G. 1992. Epithelial Na channels: function and diversity. *Annu. Rev. Physiol.* 54:51–66.

Park, C.S., C.H. Leem, Y.J. Jang, and Y.H. Shim. 2000. Vesicular transport as a new paradigm in short-term regulation of transepithelial transport. *J. Korean Med. Sci.* 15:123–132.

Paunescu, T.G., and S.I. Helman. 2001a. cAmp activation of apical membrane Cl^- channels: theoretical considerations for impedance analysis. *Biophys. J.* 81:838–851.

Paunescu, T.G., and S.I. Helman. 2001b. PGE(2) activation of apical membrane Cl^- channels in A6 epithelia: impedance analysis. *Biophys. J.* 81:852–866.

Planes, C., M. Blot-Chabaud, M.A. Matthay, S. Couette, T. Uchida, and C. Clerici. 2002. Hypoxia and β2-agonists regulate cell surface expression of the epithelial sodium channel in native alveolar epithelial cells. *J. Biol. Chem.* 277:47318–47324.

Prydz, K., S.H. Hansen, K. Sandvig, and B. van Deurs. 1992. Effects of brefeldin A on endocytosis, transcytosis, and transport to the Golgi complex in polarized MDCK cells. *J. Cell Biol.* 119:259–272.

Puri, S., C. Bachert, C.J. Fimmel, and A.D. Linstedt. 2002. Cycling of early Golgi proteins via the cell surface and endosomes upon lumenal pH disruption. *Traffic.* 3:641–653.

Reif, M.C., S.L. Troutman, and J.A. Schafer. 1986. Sodium transport by rat cortical collecting tubule. Effects of vasopressin and desoxycorticosterone. *J. Clin. Invest.* 77:1291–1298.

Rokaw, M.D., E. Sarac, E. Lechman, M. West, J. Angeski, J.P. Johnson, and M.L. Zeidel. 1996. Chronic regulation of transepithelial Na^+ transport by the rate of apical Na^+ entry. *Am. J. Physiol.* 270:C600–C607.

Rossier, B.C., S. Pradervand, L. Schild, and E. Hummler. 2002. Epithelial sodium channel and the control of sodium balance: interaction between genetic and environmental factors. *Annu. Rev. Physiol.* 64:877–897.

Rossier, B.C. 2002. Hormonal regulation of the epithelial sodium channel ENaC: N or Po? *J. Gen. Physiol.* 120:67–70.

Senyk, O., I. Ismailov, A.L. Bradford, R.R. Baker, S. Matalon, and D.J. Benos. 1995. Reconstitution of immunopurified alveolar type II cell Na^+ channel protein into planar lipid bilayers. *Am. J. Physiol.* 268:C1148–C1156.

Sheng, S., C.J. Perry, and T.R. Kleyman. 2002. External nickel inhibits epithelial sodium channel by binding to histidine residues within the extracellular domains of α and γ subunits and reducing channel open probability. *J. Biol. Chem.* 277:50098–50111.

Shimkets, R.A., R. Lifton, and C.M. Canessa. 1998. In vivo phosphorylation of the epithelial sodium channel. *Proc. Natl. Acad. Sci. USA.* 95:3301–3305.

Singh, A.K., S. Singh, D.C. Devor, R.A. Frizzell, W. Van Driessche, and R.J. Bridges. 2002. Transepithelial impedance analysis of chloride secretion. *Methods Mol. Med.* 70:129–142.

Snyder, P.M., J.C. Steines, and D.R. Olson. 2004. Relative contribution of Nedd4 and Nedd4-2 to ENaC regulation in epithelia determined by RNA interference. *J. Biol. Chem.* 279:5042–5046.

Snyder, P.M. 2000. Liddle's syndrome mutations disrupt cAMP-mediated translocation of the epithelial Na^+ channel to the cell surface. *J. Clin. Invest.* 105:45–53.

Snyder, P.M. 2002. The epithelial Na^+ channel: cell surface insertion and retrieval in Na^+ homeostasis and hypertension. *Endocr. Rev.* 23:258–275.

Snyder, P.M., D.R. Olson, F.J. McDonald, and D.B. Bucher. 2001. Multiple WW domains, but not the C2 domain, are required for inhibition of the epithelial Na^+ channel by human Nedd4. *J. Biol. Chem.* 276:28321–28326.

Sorkin, A. 2001. Internalization of the epidermal growth factor receptor: role in signalling. *Biochem. Soc. Trans.* 29:480–484.

Staub, O., H. Abriel, P. Plant, T. Ishikawa, V. Kanelis, R. Saleki, J.D. Horisberger, L. Schild, and D. Rotin. 2000. Regulation of the epithelial Na^+ channel by Nedd4 and ubiquitination. *Kidney Int.* 57: 809–815.

Tietze, C., P. Schlesinger, and P. Stahl. 1980. Chloroquine and ammonium ion inhibit receptor-mediated endocytosis of mannoseglycoconjugates by macrophages: apparent inhibition of receptor recycling. *Biochem. Biophys. Res. Commun.* 93:1–8.

Valentijn, J.A., G.K. Fyfe, and C.M. Canessa. 1998. Biosynthesis and processing of epithelial sodium channels in *Xenopus* oocytes. *J. Biol. Chem.* 273:30344–30351.

Valentijn, K., J.A. Valentijn, and J.D. Jamieson. 1999. Role of actin in regulated exocytosis and compensatory membrane retrieval: insights from an old acquaintance. *Biochem. Biophys. Res. Commun.* 266:652–661.

Van Driessche, W., R. De Vos, D. Jans, J. Simaels, P. De Smet, and G. Raskin. 1999. Transepithelial capacitance decrease reveals closure of lateral interspace in A6 epithelia. *Pflugers Arch.* 437:680–690.

Verrey, F. 1994. Antidiuretic hormone action in A6 cells: effect on apical Cl and Na conductances and synergism with aldosterone for NaCl reabsorption. *J. Membr. Biol.* 138:65–76.

Verrey, F., P. Groscurth, and U. Bolliger. 1995. Cytoskeletal disruption in A6 kidney cells: impact on endo/exocytosis and NaCl transport regulation by antidiuretic hormone. *J. Membr. Biol.* 145: 193–204.

Vinciguerra, M., G. Deschenes, U. Hasler, D. Mordasini, M. Rousselot, A. Doucet, A. Vandewalle, P.Y. Martin, and E. Feraille. 2003. Intracellular Na^+ controls cell surface expression of Na,K-ATPase via a cAMP-independent PKA pathway in mammalian kidney collecting duct cells. *Mol. Biol. Cell.* 14:2677–2688.

Weber, W.M., H. Cuppens, J.J. Cassiman, W. Clauss, and W. Van Driessche. 1999. Capacitance measurements reveal different pathways for the activation of CFTR. *Pflugers Arch.* 438:561–569.

Weisz, O.A., J.M. Wang, R.S. Edinger, and J.P. Johnson. 2000. Noncoordinate regulation of endogenous epithelial sodium channel (ENaC) subunit expression at the apical membrane of A6 cells in response to various transporting conditions. *J. Biol. Chem.* 275: 39886–39893.

Weng, K., and J.B. Wade. 1994. Effect of brefeldin A on ADH-induced transport responses of toad bladder. *Am. J. Physiol.* 266: C1069–C1076.

Wills, N.K., R.K. Purcell, and C. Clausen. 1992. Na^+ transport and impedance properties of cultured renal (A6 and 2F3) epithelia. *J. Membr. Biol.* 125:273–285.